JACS
JOURNAL OF THE AMERICAN CHEMICAL SOCIETY
Article
pubs.acs.org/JACS

Stability and Dynamic Processes in 16VE Iridium(III) Ethyl Hydride and Rhodium(I) σ-Ethane Complexes: Experimental and Computational Studies

Marc D. Walter,[†,‡] Peter S. White,[†] Cynthia K. Schauer,[†] and Maurice Brookhart*[,†]

[†]Department of Chemistry, University of North Carolina at Chapel Hill, Chapel Hill, North Carolina 27599-3290, United States
[‡]Institut für Anorganische und Analytische Chemie, Technische Universität Braunschweig, D-38106 Braunschweig, Germany

Supporting Information

ABSTRACT: Iridium(I) and rhodium(I) ethyl complexes, (PONOP)M(C_2H_5) (M = Ir (**1-Et**), Rh (**2-Et**)) and the iridium(I) propyl complex (PONOP)Ir(C_3H_7) (**1-Pr**), where PONOP is 2,6-(tBu$_2$PO)$_2$C$_5$H$_3$N, have been prepared. Low-temperature protonation of the Ir complexes yields the alkyl hydrides, (PONOP)Ir(H)(R) (**1-(H)(Et)**$^+$ and **1-(H)(Pr)**$^+$), respectively. Dynamic ^{1}H NMR characterization of **1-(H)(Et)**$^+$ establishes site exchange between the Ir−*H* and Ir−C*H*$_2$ protons ($\Delta G_{exH}^{\ddagger}$(−110 °C) = 7.2(1) kcal/mol), pointing to a σ-ethane intermediate. By dynamic ^{13}C NMR spectroscopy, the exchange barrier between the α and β carbons ("chain-walking") was measured ($\Delta G_{exC}^{\ddagger}$(−110 °C) = 8.1(1) kcal/mol). The barrier for ethane loss is 17.4(1) kcal/mol (−40 °C), to be compared with the reported barrier to methane loss in **1-(H)(Me)**$^+$ of 22.4 kcal/mol (22 °C). A rhodium σ-ethane complex, (PONOP)Rh(EtH) (**2-(EtH)**$^+$), was prepared by protonation of **2-Et** at −150 °C. The barrier for ethane loss ($\Delta G_{dec}^{\ddagger}$(−132 °C) = 10.9(2) kcal/mol) is lower than for the methane complex, **2-(MeH)**$^+$, ($\Delta G_{dec}^{\ddagger}$(−87 °C) = 14.5(4) kcal/mol). Full spectroscopic characterization of **2-(EtH)**$^+$ is reported, a key feature of which is the upfield signal at −31.2 ppm for the coordinated CH_3 group in the ^{13}C NMR spectrum. The exchange barrier of the hydrogens of the coordinated methyl group is too low to be measured, but the chain-walking barrier of 7.2(1) kcal/mol (−132 °C) is observable by ^{13}C NMR. The coordination mode of the alkane ligand and the exchange pathways for the Rh and Ir complexes are evaluated by DFT studies. On the basis of the computational studies, it is proposed that chain-walking occurs by different mechanisms: for Rh, the lowest energy path involves a η^2-ethane transition state, while for Ir, the lowest energy exchange pathway proceeds through the symmetrical ethylene dihydride complex.

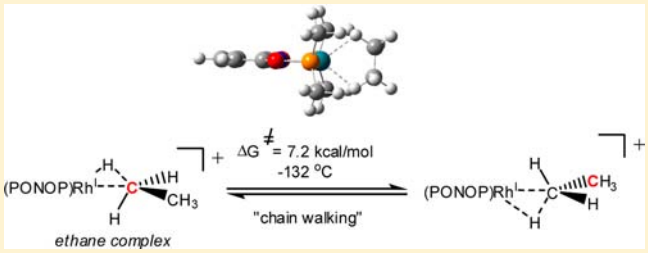

INTRODUCTION

Direct and selective functionalization of alkanes—as the cheapest and most abundant feedstock for value-added organic molecules—is one of the most active areas of homogeneous catalysis. These efforts are mainly driven by the huge potential economic impact. However, the C−H bond dissociation enthalpies of alkanes are quite high, and further functionalization, e.g., by selective oxidation, is hampered by undesirable overoxidation attributable to the fact that the products of alkane oxidations are typically more reactive than the starting alkane itself.[1−3] Despite these difficulties, the last several decades have brought significant progress, and numerous promising transition-metal systems for alkane functionalization have emerged.[4−17] Highly topical areas of alkane oxidation reactions include alkane dehydrogenation and oxygen transfer.[18−21] Several different metal complexes are competent catalysts for the dehydrogenation of alkanes to olefins, and mechanistic studies have provided deep insight into the C−H activation and β-hydride elimination steps.[22,23]

The worldwide abundance of methane and the potential value of converting it to simple oxidation products made the Pt(II)-catalyzed conversions of methane to methanol,[24] to methyl bisulfate,[25] and to acetic acid[26] the most thoroughly studied reactions for methane functionalization. In the groundbreaking work by Shilov, the Pt(II) species, $[PtCl_4]^{2-}$, was used as the catalyst and $[PtCl_6]^{2-}$ (Pt(IV)) served as the sacrificial oxidant to convert methane into methanol in aqueous solution.[27] Over the last 30 years the mechanism of Pt(II)-catalyzed alkane oxidations has been thoroughly investigated, and a variety of model systems have provided more detailed insights into the key C−H bond activation step.[28−30] The now generally accepted mechanism for this electrophilic methane activation process is shown in Figure 1 and includes: (1) CH_4 coordination to a Pt(II) center to generate a σ-alkane complex; (2) oxidative cleavage of the C−H bond to afford a five-coordinate Pt(IV) methyl hydride species; and (3) deprotonation to generate a Pt(II) methyl complex. However, neither the Pt(II) σ-methane complex nor the five-coordinate Pt(IV) methyl hydride have been directly observed, but their existence

Received: August 8, 2013
Published: September 20, 2013

   dx.doi.org/10.1021/ja4079539 | J. Am. Chem. Soc. 2013, 135, 15933−15947

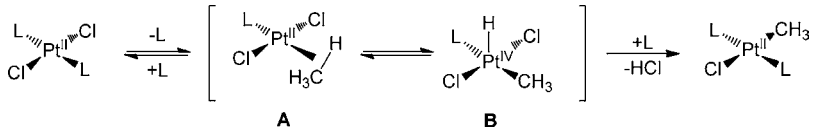

Figure 1. Mechanism for the electrophilic activation of methane by platinum(II).

has been inferred from mechanistic and computational studies on model systems.[2,31−34]

The structure, stability, and properties (e.g., acidity) of σ-alkane complexes and the selectivity of binding to various C−H bonds can all play a key role in the kinetics and selectivity of carbon−hydrogen bond activation and functionalization regardless of whether they proceed via an oxidative cleavage or a σ-CAM mechanism.[29,35−38] To this end, it is of interest to generate and characterize, to the extent possible, σ-alkane complexes.

However, the major challenge in the characterization of σ-alkane complexes is that the strong nonpolar C−H σ-bond is only a weak donor, and steric repulsions between the alkyl group and the metal center impede a close approach of the alkane to the metal.[39] Originally, methane complexes were observed and characterized by IR spectroscopy via photodissociation of CO from $M(CO)_6$ (M = Cr, Mo, and W) in methane matrices at very low temperature (12 K).[40,41] Sophisticated techniques such as fast time-resolved infrared (TRIR) spectroscopy have been developed and applied in solution phase to these highly reactive systems.[42,43] A systematic study of related metal carbonyl alkane complexes by TRIR spectroscopy showed an increased lifetime of these σ-alkane complexes on going both across and down Groups 5−7.[44] The increased stability of this class of compounds subsequently allowed their characterization with ^{1}H NMR spectroscopy.[44−53] Photolysis of $(C_5H_5)Re(CO)_3$ in cyclopentane at 180 K yielded the corresponding alkane complex, which was the first alkane complex to be characterized by ^{1}H NMR spectroscopy.[48] A still not completely resolved issue is the question of site-selectivity in the formation of σ-alkane complexes, e.g., photolysis of $(i\text{-}PrC_5H_4)Re(CO)_3$ in pentane gives the C1-, C2-, and C3-bound isomers in a relative ratio of 6:6:3, compared to the statistical ratio of 6:4:2, which suggests a slight thermodynamic preference of the CH_2 sites over CH_3. In addition, the three isomers slowly interconvert intramolecularly (∼1−10 s^{-1}) at −100 °C.[50] In contrast, photolysis of the lighter homologue $(C_5H_5)Mn(CO)_3$ in butane shows significantly reduced lifetimes of the σ-alkane complexes and little selectivity between C1 and C2 isomers,[51] while after photolysis of $(C_6Et_6)W(CO)_3$ in pentane only the C1 isomer is detected.[53] While there is strong evidence of intermolecular metal−alkane interactions in solution, alkane complexes usually defy isolation and solid-state structural characterization. Two X-ray structures have been published of complexes in which the alkane solvent is located in the proximity of metal centers, but no alkane σ-complex is observed in solution.[54,55] Only recently, a new synthetic approach to transition-metal alkane complexes via a single crystal-to-single crystal transformation was reported by a simple gas−solid reaction. This method allowed the structural determination (by X-ray diffraction) of a norbornane which is σ-bound through two σ-C−H bonds to a Rh(I) metal center.[56]

We recently reported the isolation of an unusually stable five-coordinate 16VE Ir(III) hydrido methyl cation, $[(PONOP)Ir(H)(CH_3)][B(Ar_F)_4]$ {where PONOP is 2,6-$(tBu_2PO)_2C_5H_3N$; *t*Bu is $C(CH_3)_3$; and $B(Ar_F)_4$ is $B[3,5\text{-}(F_3C)_2C_6H_3]_4$}, which is isoelectronic with the Pt(IV) methyl hydride species **B** proposed in the Shilov cycle.[57] Additionally, rapid interchange between the Ir−H and Ir−CH_3 protons was observed and established reversible formation of a σ-methane complex. DFT calculations suggested that the $[(PONOP)Ir(H)(CH_3)]^+$ ground state lies only ∼5 kcal/mol below the $[(PONOP)Ir(\sigma\text{-}CH_4)]^+$ complex.[58] However, the small ground-state free energy difference between $[(PONOP)Ir(H)(CH_3)]^+$ and $[(PONOP)Ir(\sigma\text{-}CH_4)]^+$ and the substantial binding energy of the σ-methane motivated us to investigate the Rh analogue in which the Rh(I) oxidation state should be modestly stabilized relative to the Rh(III) state. Indeed, protonation of $[(PONOP)Rh(CH_3)]$ at low temperature permitted the observation and full characterization by NMR spectroscopy of a relatively long-lived σ-methane complex, $[(PONOP)Rh(CH_4)][B(Ar_F)_4]$. This complex is isoelectronic with the Pt(II) σ-methane complexes **A** (Figure 1), which are postulated as intermediates in the Shilov-type oxidations of methane.[58] In our synthetic approach, the metal σ-methane complex is generated by protonation directly at the M−CH_3 bond. The cationic charge of the complex gives rise to a significantly increased lifetime of the corresponding σ-alkane complex compared to the neutral complexes. However, even weakly coordinating solvents such as $CHCl_2F$ bind more strongly to the cationic metal center than the corresponding alkane, and therefore loss of bound alkane is an irreversible process.[58]

Encouraged by these initial results, it was desirable to expand our studies to other alkane complexes using the same methodology, i.e., protonation of their alkyl precursors, and to investigate their dynamics and reactivity.[59] Experiments can be envisioned which will lend insight into how rapidly the metal complex can migrate along the alkane chain and which alkane isomers are thermodynamically favored. These can then be compared to previous studies on neutral complexes such as $(C_5Me_5)Rh(PMe_3)(^{13}CH_2CH_3)(D)$[60] and Tp′Rh(L)$(CH_2CH_2CH_2CH_3)(D)$[61] and cationic complexes such as {(1,4,7-triazacyclononane)Rh(alkyl)D$[P(OMe)_3]$}$^+$,[62] which provided indirect evidence for the formation of alkane complexes in which the metal migrates along the alkane chain prior to reductive elimination.[63] Herein, we report on (PONOP)M (M = Ir/Rh) complexes with longer alkyl chains including the observation of a cationic Rh(I) σ-ethane complex. The dynamics of chain-walking in this Rh(I) σ-ethane complex and the analogous Ir(I) ethyl hydride complex are explored by DFT calculations and compared to the experimental data.

RESULTS AND DISCUSSION

Synthesis and Characterization of (PONOP)M(C_2H_5) (M = Ir (1-Et), Rh (2-Et)). The iridium(I) and rhodium(I) ethyl complexes, (PONOP)M(C_2H_5) (M = Ir (**1-Et**), Rh (**2-Et**)), were prepared by addition of $MgEt_2$ to the corresponding halide precursors (Scheme 1). The reaction needs to be carefully monitored since the conversion proceeds slowly. Similar to (PONOP)IrCH_3 (**1-Me**), the synthesis of **1-Et** required harsher reaction conditions than the preparation of **2-Et**.

dx.doi.org/10.1021/ja4079539 | J. Am. Chem. Soc. 2013, 135, 15933−15947

Scheme 1. Synthesis of 1-Et, 1-Pr, and 2-Et

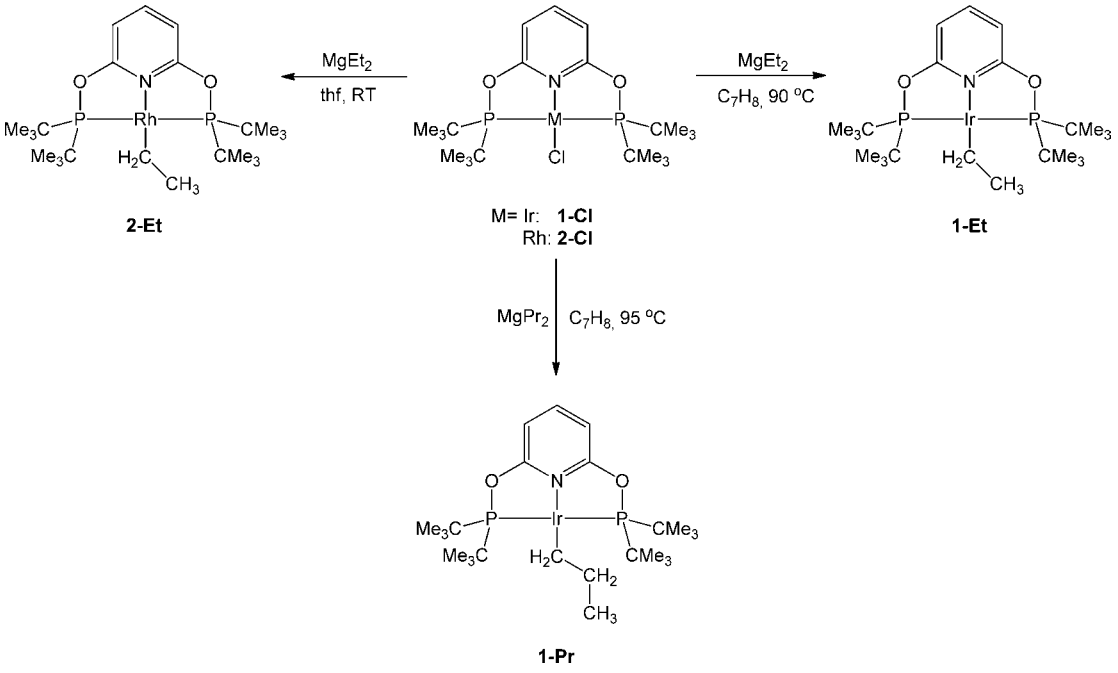

Several additional alkylating reagents such as LiEt and $ZnEt_2$ and reaction conditions were investigated; however, at ambient temperature no reaction occurred, while at elevated temperature significant degradation accompanied the formation of insoluble material. The cleanest conversion was obtained using $MgEt_2$. Complexes **1-Et** and **2-Et** were characterized by NMR spectroscopy and elemental analysis and in the case of **2-RhEt** by single crystal X-ray diffraction. ^{1}H NMR spectra of **1-Et** and **2-Et** are consistent with a molecular C_{2v} symmetry (see Experimental Section for details). The $^{31}P\{^1H\}$ NMR spectra of **1-Et** and **2-Et** display a singlet at δ 185.7 and a doublet at δ 197.6 ($^1J_{P-Rh}$ = 183 Hz), respectively. The $^{31}P\{^1H\}$ NMR chemical shifts of **1-Et** and **2-Et** are shifted downfield relative to that of **1-Cl** and **2-Cl**, respectively (see SI for details, Table S1).

The solid-state structure of **2-Et** is depicted in Figure 2, and selected bond distances and angles are given in the figure caption. The geometry around the Rh center is best described as square planar, and the ethyl substituent is situated nearly orthogonal to that of the backbone of the pyridine ring. No β-agostic interactions were observed.

Given the unusual stability of **1-Et**, it was of interest to explore if the neutral complex **1-Et** undergoes thermally induced β-hydride elimination to form the monohydride complex **1-H**. The β-hydride elimination proceeds cleanly at 134 °C with a first-order rate constant of $k = 2.8(1) \times 10^{-5}$ s^{-1}, corresponding to a barrier for ethylene loss of $\Delta G^{\ddagger}$ = 32.6(1) kcal/mol.[64] Product **1-H** was characterized by multinuclear NMR spectroscopy (Table S1 and see Experimental Section for details). The significant chemical shift separation between **1-Et** and **1-H** in the $^{31}P\{^1H\}$ NMR spectrum made it possible to measure the rate of this conversion. In the ^{1}H NMR spectrum, the disappearance of the ethyl moiety of **1-Et** is accompanied by the formation of C_2H_4 and **1-H** (Scheme 2).

Protonation of 1-Et and 2-Et: Characterization of the (PONOP)Ir(H)(Et)$^+$ Cation (1-(H)(Et)$^+$). Cation **1-(H)(Et)**$^+$ may be generated by addition of acids such as $[H(OEt_2)_2][B(Ar_F)_4]$ or $HN(SO_2CF_3)_2$ to **1-Et** in $CDCl_2F$ at −100 °C

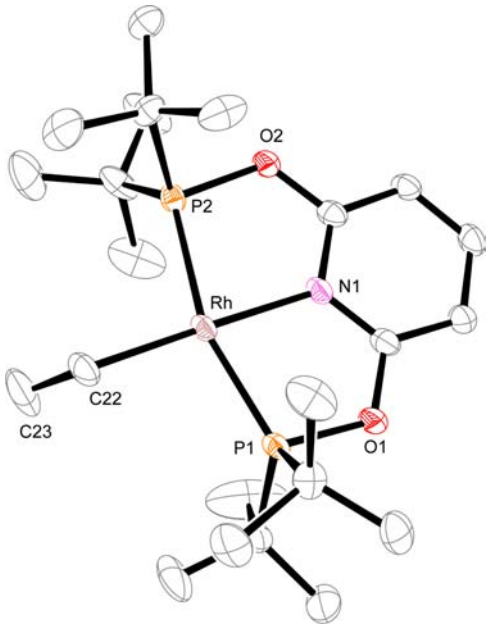

Figure 2. ORTEP diagram of **2-Et** (50% probability ellipsoids). Selected bond distances (Å) and angles (°): Rh−N1, 2.066(2); Rh−C22, 2.112(3); C22−C23, 1.505(5); Rh−P1, 2.2465(7); Rh−P2, 2.2301(7); Rh−C22−C23, 116.5(2).

(see Experimental Section and SI for details). We preferred $HN(SO_2CF_3)_2$ as acid in the case of **1-Et** to simplify the NMR spectra and to avoid overlapping NMR resonances (Scheme 3). We were initially rather surprised to find that, in contrast to **1-(H)(Me)**$^+$, the ethyl hydride complex **1-(H)(Et)**$^+$ displayed a significantly reduced thermal stability which prevented the isolation of cationic **1-(H)(Et)**$^+$. While the complex undergoes ethane elimination instantaneously at ambient temperature, the half-life of this process is ∼2.5 h at −40 °C. This observation made it necessary to generate the protonated species at low temperature and to ensure efficient mixing of both reactants

dx.doi.org/10.1021/ja4079539 | J. Am. Chem. Soc. 2013, 135, 15933−15947

Scheme 2. β-Hydride Elimination in 1-Et

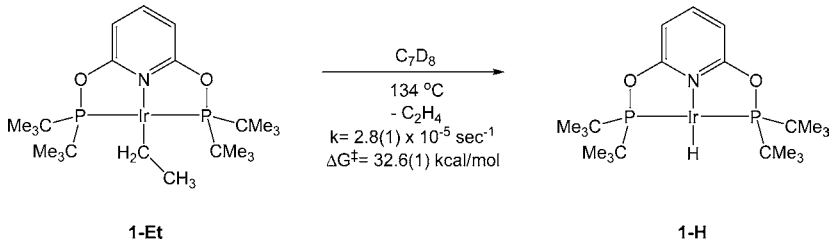

Scheme 3. Generation of 1-(H)(Et)$^+$ and 1-(EtH)$^+$

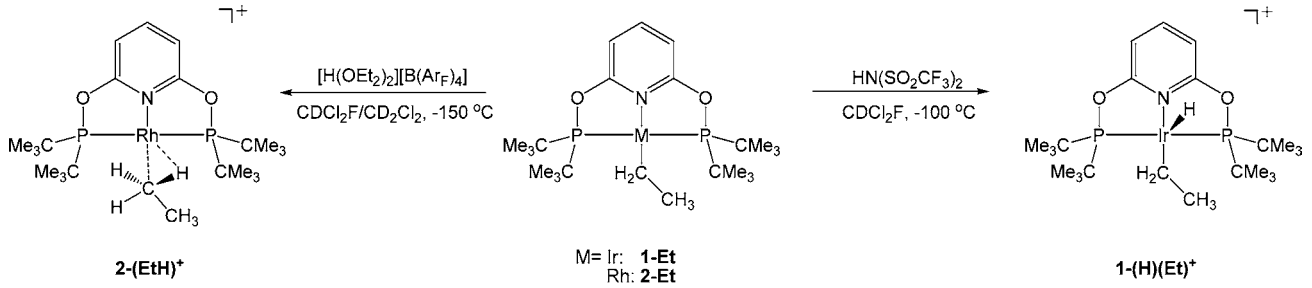

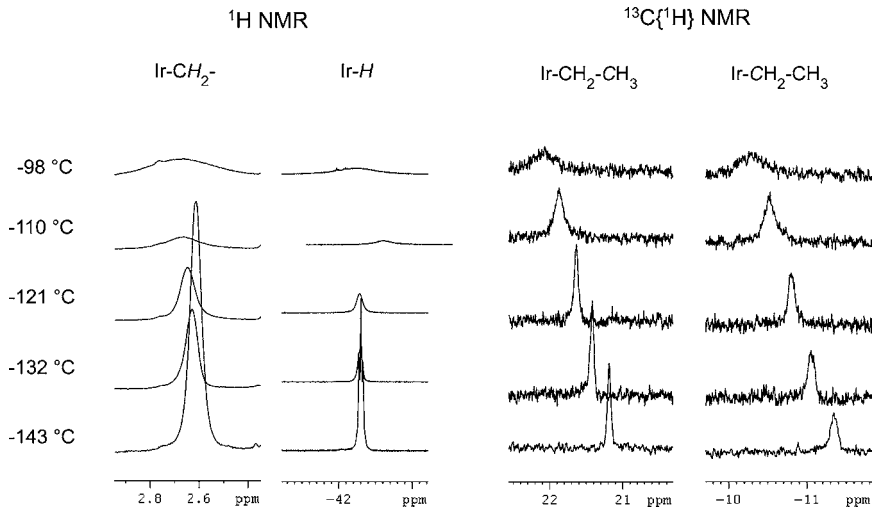

Figure 3. Temperature dependence of selected ^{1}H and ^{13}C{^{1}H} resonances undergoing Ir−H/Ir−CH_2R and C_α−C_β site exchange.

without warming the sample. Recently, Jutzi and co-workers described a method to generate temperature labile species directly in an NMR tube.[65] While this procedure certainly deserves proper attention, we would like to advocate a long-known, but rarely used, simple device originally introduced by Winstein and co-workers, which allows for precise temperature control as low as −150 °C.[66] Interested readers may refer to the SI for a more detailed description of our modified version of this device.

The product of ethane loss was tentatively assigned as the iridium(I) solvate cation, $[(PONOP)Ir(CDCl_2F)]^+$. Free ethane was detected concomitant with and roughly proportional to the formation of $[(PONOP)Ir(CDCl_2F)]^+$. This degradation was conveniently monitored by ^{31}P{^{1}H} NMR spectroscopy to give a first-order rate constant of k = 8.0(1) × 10^{-5} s^{-1} at −40 °C corresponding to a barrier of ethane loss of $\Delta G^{\ddagger}$ = 17.4(1) kcal/mol (see SI for details). For comparison, the barrier of methane elimination in **1-(H)(Me)**$^+$ is $\Delta G^{\ddagger}$ = 22.4(2) kcal/mol. The decreased stability of **1-(H)(Et)**$^+$ by 5 kcal/mol may be attributed to the increased strain imposed between the large ethyl group and the sterically demanding −CMe_3 groups. Cation **1-(H)(Et)**$^+$ was characterized by multinuclear, low-temperature NMR spectroscopy. At −143 °C in CD_2Cl_2 solution the ^{1}H NMR spectrum of **1-(H)(Et)**$^+$ displays a triplet resonance at δ −42.30 ($^2J_{P-H}$ = 13.6 Hz) assigned to the Ir−H and a broad resonance at δ 2.65 assigned to the Ir−CH_2 moiety. The resonance attributed to the Ir−CH_2CH_3 is masked by the broad resonance corresponding to the two sets of inequivalent −CMe_3 groups. Warming of the sample to −121 °C results in substantial broadening of both the Ir−H and Ir−CH_2 resonances along with a small change in the chemical shifts to δ −42.28 and 2.67, respectively (Figure 3). The rate of site exchange between the Ir−H and Ir−CH_2 positions was examined in a selectively ^{1}H{^{31}P}-decoupled NMR spectrum by line shape analysis.[67] At −110 °C in $CDCl_2F$ solvent, a rate constant of 725(10) s^{-1} was observed for the Ir−H and Ir−CH_2 exchange which corresponds to a barrier of 7.2(1) kcal/mol for the interchange of iridium−hydride and iridium−methylene protons by reductive coupling and oxidative cleavage.

dx.doi.org/10.1021/ja4079539 | J. Am. Chem. Soc. 2013, 135, 15933−15947

The observed site exchange between the Ir−*H* and Ir−C*H*$_2$ protons points to a reversible σ-ethane complex formation. It is interesting to note that the barrier for this exchange process in **1-(H)(Et)**$^+$ is reduced by ∼2 kcal/mol compared to **1-(H)(Me)**$^+$ ($\Delta G^{\ddagger}$ = 9.3(4) kcal/mol). The intermediacy of a reversible σ-ethane complex posed the question as to how rapidly the α-CH_2 and β-CH_3 sites of the ethyl ligand exchange (δ −11.0 for α-CH_2 and δ +21.5 for β-CH_3). Variable temperature (VT) $^{13}C\{^1H\}$ NMR spectroscopy was used to answer this question. On warming, both resonances broaden significantly, and the rate of site exchange between both sites was examined by line shape analysis (Figure 3).[67] At −110 °C in $CDCl_2F$ solvent, a rate constant of 57(2) s^{-1} was observed corresponding to an exchange barrier of 8.1(1) kcal/mol. This exchange can be envisioned to proceed either via cationic [(PONOP)Ir(H)$_2$-(C_2H_4)]$^+$ or [(PONOP)Ir(σ-C_2H_6)]$^+$ intermediates (Figure 4).

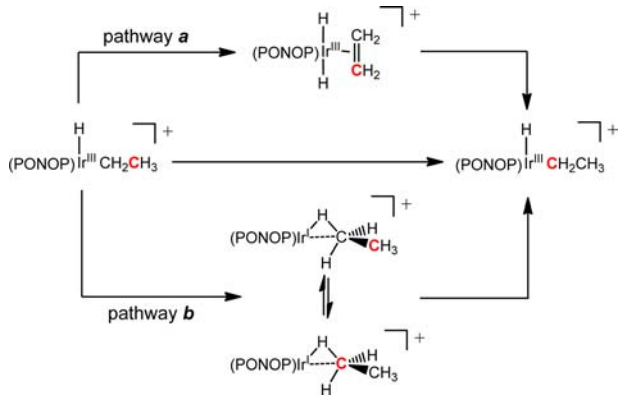

Figure 4. Two alternative pathways for C_α−C_β site exchange (a) β-hydride elimination, re-insertion and (b) chain-walking via the σ-ethane complex.

However, neither intermediate was detected by NMR spectroscopy. Experiments directed at further probing the mechanism of the exchange are described below, and the mechanism of exchange is explored in detail in the Computational Results section. The observed exchange processes and the corresponding barriers for the Ir ethane system are summarized in Figure 5.

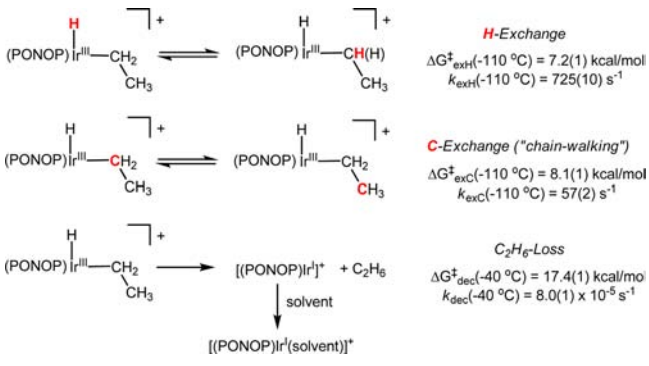

Figure 5. Dynamic processes and barriers for **1-(H)(Et)**$^+$.

Preparation of 1-Pr and Its Protonation. A new experiment was designed to further probe the mechanism of α, β site exchange, which led to the synthesis of the iridium propyl complex, **1-Pr**. The synthesis of **1-Pr** was accomplished in a similar manner to **1-Et** but at a lower temperature. Complex **1-Pr** was characterized by multidimensional NMR, combustion analysis, and single crystal X-ray diffraction (see Experimental Section for details). The molecular structure is shown in Figure 6, and selected bond distances and angles are given in the Figure caption.

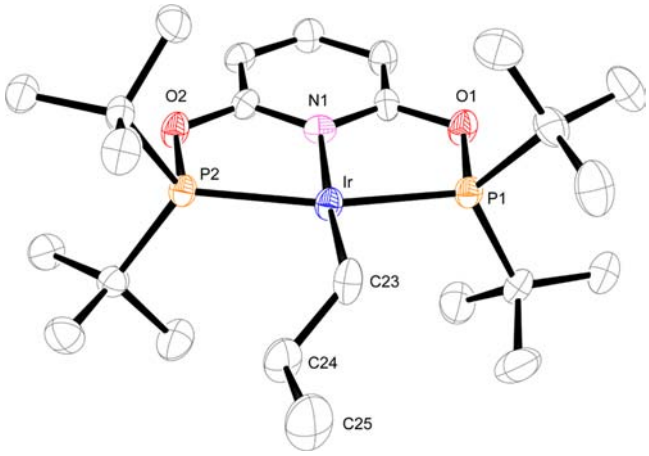

Figure 6. ORTEP diagram of **1-Pr** (50% probability ellipsoids). Selected bond distances (Å) and angles (°): Ir−N1, 2.043(5); Ir−C22, 2.123(6); C22−C23, 1.490(9); C24−C25, 1.535(10); Ir−P1, 2.2313(13); Ir−P2, 2.2413(13); Ir−C22−C23, 121.0(4).

Complex **1-Pr** was protonated with an excess of $HN(SO_2CF_3)_2$ in $CDCl_2F$ at −100 °C. The resulting cationic **1-(H)(Pr)**$^+$ shows a slightly enhanced thermal stability compared to **1-(H)(Et)**$^+$, and propane is eliminated with a barrier of 18.6(2) kcal/mol, which is ∼1.0 kcal/mol higher than for **1-(H)(Et)**$^+$ (see SI for details). The origin of this increased stability is not obvious, but it may be attributed to the formation of weakly stabilizing hydrophobic interactions between the propyl chain and the *t*Bu groups. Despite the slightly increased barrier to propane dissociation, the complex is thermally unstable above −40 °C, and P−O cleavage in addition to propane loss has been observed. In a direct comparison of the exchange barrier between the Ir−*H* and Ir−C*H*$_2$R moieties, a slightly reduced barrier of $\Delta G^{\ddagger}$ = 6.9 kcal/mol in comparison to **1-(H)(Et)**$^+$ was determined based on line broadening experiments at −110 °C (see SI for details). Unfortunately, no significant line broadening in the $^{13}C\{^1H\}$ NMR was observed up to −40 °C, preventing the barrier for end-to-end scrambling to be determined. However, a lower limit of $\Delta G^{\ddagger}$ > 12.6 kcal/mol for this barrier to chain-walking can be estimated.

A ^{2}H-labeled propyl moiety was employed to carry out an experiment that potentially allows differentiation between the two alternative pathways for C_α−C_β scrambling. Introducing ^{2}H labels in the 3-position of the (PONOP)Ir(H)($CH_2CH_2CD_3$)$^+$ and monitoring the scrambling of the ^{2}H along the propyl chain by $^2H\{^1H\}$ NMR spectroscopy would provide a more in-depth understanding of the mechanism. For the case of exchange proceeding through a σ-propane intermediate, ^{2}H labels are expected in the 1- and 3-positions, whereas for a dihydride propene intermediate, ^{2}H labels should be found in all three positions of the propyl group. In an attempt to observe ^{2}H scrambling (on a laboratory time scale), the sample was kept at −40 °C for a prolonged period of time. Unfortunately alkane loss is observed before any ^{2}H scrambling occurs, so no information about the mechanism of scrambling could be gleaned.

dx.doi.org/10.1021/ja4079539 | J. Am. Chem. Soc. 2013, 135, 15933−15947

Characterization of the (PONOP)Rh(EtH)$^+$ Cation (2-(EtH)$^+$). In our previous work, a combination of the small free energy difference between the iridium(III) methyl hydride complex and the iridium(I) methane adduct, together with the ease of reduction of rhodium relative to its iridium congener, led to the observation and full solution characterization of a relative long-lived rhodium σ-methane complex.[58] A σ-ethane complex seemed attainable, and the observation of exchange between the $\alpha-$ and β-CH_3 sites would provide insight into chain-walking in **2-(EtH)**$^+$. However, the generation and observation of **2-(EtH)**$^+$ presented a major challenge for two reasons: (1) **2-Et** is not very soluble in pure $CDCl_2F$ solvent, and (2) the thermal stability of **2-(EtH)**$^+$ is significantly lower when compared to **2-(MeH)**$^+$, which makes precise temperature control during handling and mixing an absolute necessity. Complex **2-(EtH)**$^+$ was prepared by protonation of **2-Et** with $[H(OEt_2)_2][B(Ar_F)_4]$ in $CDCl_2F$/CD_2Cl_2 solution at −150 °C. Generation at this temperature was necessary as the σ-ethane complex **2-(EtH)**$^+$ loses ethane extremely rapidly with an approximate half-life of ∼5.5 h at −132 °C. The product of ethane extrusion was assigned as the rhodium(I) solvated cation, [(PONOP)Rh(solv)]$^+$ (solv = CD_2Cl_2 and $CDCl_2F$).[58] Free ethane was detected along with and roughly proportional to the formation of [(PONOP)Rh(solv)]$^+$. At −143 °C **2-(EtH)**$^+$ shows a doublet in the $^{31}P\{^1H\}$ NMR spectrum at δ 208.1 ($^1J_{RhP}$ = 136 Hz) compared to δ 197.6 ($^1J_{RhP}$ = 183 Hz) for **2-Et**. The rate of loss of ethane was monitored by $^{31}P\{^1H\}$ NMR spectroscopy and the first-order rate constant was calculated to be $k = 3.4(2) \times 10^{-5}$ s^{-1} at −132 °C, corresponding to a barrier of ethane loss of $\Delta G^{\ddagger}$ = 10.9(2) kcal/mol (see SI for details). It is instructive to compare this value to the barrier of methane extrusion in **2-(MeH)**$^+$ of 14.5(4) kcal/mol.[58] Interestingly, exchanging a methyl for an ethyl ligand in the (PONOP)M (M = Ir and Rh) systems leads to a similar kinetic destabilization of the corresponding protonated species of ∼4−5 kcal/mol. As outlined above, steric factors are the most likely explanation for this observation. The wedge imposed by the pincer CMe_3 groups forms a perfect cavity for the small and nearly spherical CH_4 ligand, while an additional substrate methyl group in the corresponding σ-ethane intermediate cannot be readily accommodated into this severely constrained coordination environment.

Despite the low stability of the σ-ethane complex, **2-(EtH)**$^+$, we succeeded in fully characterizing this species by a series of low-temperature 1D- and 2D-NMR experiments. The $^{13}C\{^1H\}$ NMR of **2-(EtH)**$^+$ at −143 °C exhibits two resonances at δ −31.6 ($^1J_{CH}$ = 124 Hz) and 11.7 ($^1J_{CH}$ = 127 Hz) corresponding to the two CH_3 groups of the σ-C_2H_6 ligand. Both resonances are singlets with a line width at half-height ($\nu_{1/2}$) of 10.9 and 7.5 Hz, respectively, compared to $\nu_{1/2}$ = 2.5 Hz for free ethane (δ 7.0) in solution. The line width of bound ethane may be attributed to unresolved small ^{103}Rh- or ^{31}P couplings. Such small couplings also indicate a reduced interaction of the σ-ethane and the (PONOP)Rh^I fragment especially when contrasted to the coupling constants ($^1J_{RhC}$ = 25.7 Hz and $^2J_{PC}$ = 9.7 Hz) for the α-CH_2 position in the precursor **2-Et**. Since we did not prepare the ^{13}C-labeled isotopologue of **2-(EtH)**$^+$, the $^1J_{CH}$ coupling constants were determined by a decoupled gradient-HSQC experiment,[68] and both resonances have been unambiguously identified as CH_3 groups by DEPT experiments. The resonance at δ −31.6 is shifted dramatically upfield relative to **2-Et** and **1-(H)(Et)**$^+$ which exhibit $^{13}C\{^1H\}$ NMR resonances at −9.4 and −11.0 ppm, respectively. Also informative is the comparison with the bound methane resonance in **2-(MeH)**$^+$ at δ −41.7. The observed downfield shift by ∼10 ppm in the ethane complex is in good agreement with prediction based on the empirical ^{13}C NMR increment system and *ab initio* calculations on simple alkanes.[69,70] The observed $^1J_{CH}$ coupling constant of 124 Hz for the agostic-CH_3 group in **2-(EtH)**$^+$ is comparable to that of free ethane in $CDCl_2F$ solution (128 Hz) and substantially larger than the expected average coupling constant for a rapidly fluxional transition-metal ethyl hydride complex of ∼85 Hz.

The ^{1}H NMR spectrum of **2-(EtH)**$^+$ at −143 °C exhibited the number of resonances expected for a C_{2v} symmetric molecule with two broad resonances at δ −0.83 and +1.13, and the COSY experiment showed the expected cross-peaks for the σ-ethane fragment. The HSQC NMR experiment indicated that these resonances correlate to the $^{13}C\{^1H\}$ NMR resonances at δ −31.6 and 11.7, respectively. No detectable phosphorus−hydrogen coupling was observed, and selective decoupling of the ^{31}P resonance (δ 208.1) did not result in an observable change in the line width for the resonance at δ −0.83.

Similar to **1-(H)(Et)**$^+$ it was of interest to investigate the exchange process between the α-C and β-C sites of **2-(EtH)**$^+$ which resonate at δ at −31.6 and 11.7 at −143 °C, respectively. For this purpose we employed VT $^{13}C\{^1H\}$ NMR spectroscopy. On warming, both resonances broaden significantly and the rate of site exchange between both sites was examined by line shape analysis.[67] At −132 °C in $CDCl_2F/CD_2Cl_2$ solvent, a rate constant of 25(1) s^{-1} was observed corresponding to an exchange barrier of 7.2(1) kcal/mol. Dynamic processes and associated barriers are summarized in Figure 7.

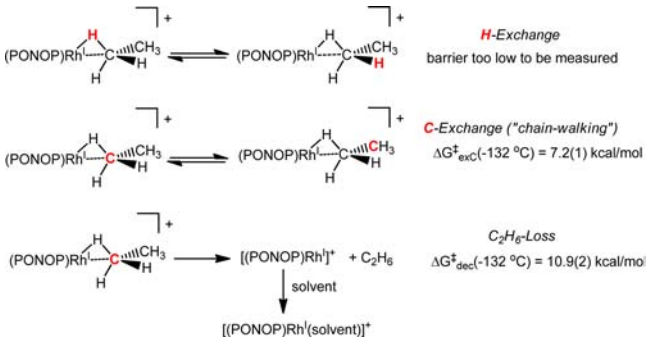

Figure 7. Dynamic processes and barriers for **2-(EtH)**$^+$.

■ COMPUTATIONAL RESULTS

Computational studies have provided valuable insights into the bonding of alkanes to transition-metal complexes.[39,59,71−73] To gain additional information on the binding mode of the σ-ethane ligands, the energy of the ethyl hydride complex relative to the ethane complex in the rhodium and iridium systems, and the experimentally observed rates of exchange, a DFT study was undertaken using the PBE0 functional (for details, see Computational Details in the Experimental Section).

Two views of the optimized singlet ground-state structure for the rhodium ethane complex **(2-EtH)**$^+$ are shown in Figure 8a,b, and a comparison of the key structural parameters of the ethane and methane complexes is given in Figure 8c,d, respectively. The C−C bond of the ethane ligand adopts a nearly

dx.doi.org/10.1021/ja4079539 | J. Am. Chem. Soc. 2013, 135, 15933−15947

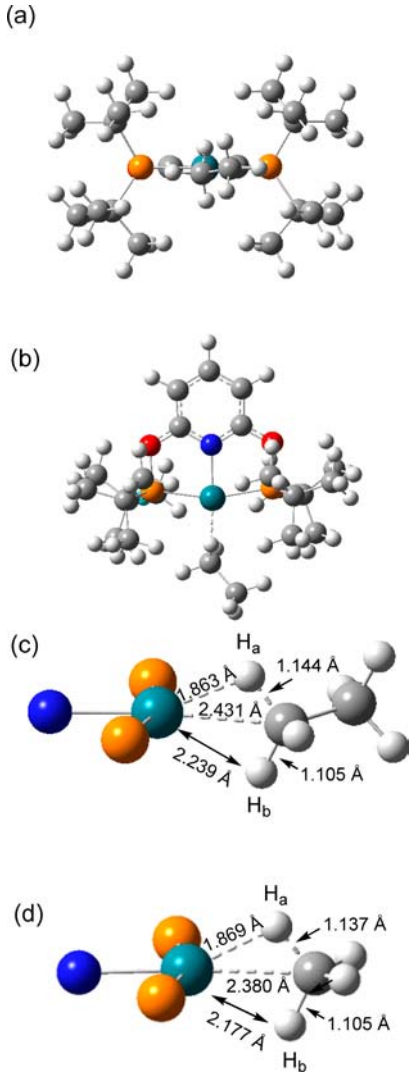

Figure 8. (a) View in the plane of the pincer ligand of the calculated structure of the rhodium ethane complex, **2-Et**. (b) View perpendicular to the plane of the pincer ligand of the calculated structure of the rhodium ethane complex, **2-Et**. (c) Truncated structure showing structural parameters for the coordinated ethane ligand in **2-Et**. (d) Truncated structure showing structural parameter for the corresponding methane complex.

parallel orientation with respect to the plane of the pincer ligand, with the terminal methyl group positioned between the *t*Bu groups above and below the plane. As previously observed for the methane complex,[58] an unsymmetrical interaction between rhodium and the ethane ligand is observed, with only one C−H bond coordinated to the metal (η^2-C,H; Figure 8c), as signified by the relative values of Rh−H_a (1.863 Å) and Rh−H_b (2.239 Å) as well as the corresponding C−H distances (1.144 and 1.105 Å for H_a and H_b, respectively). The coordinated C−H_a bond is oriented perpendicular to the plane of the pincer ligand. Comparing Figure 8c and 8d, the most significant structural difference between the methane and ethane complexes is the longer Rh−H_b and Rh−C distances for the coordinated ethane ligand. While a single C−H bond is coordinated in the lowest energy structure, the potential energy surface associated with exchange of the coordinated hydrogens is essentially flat.

For the calculation of reaction pathways in the system, it was necessary to employ a trimmed ligand in which the *t*Bu groups were replaced by Me groups (PONOP-trim). Shown in Figure 9 is a comparison of the structural parameters for the Rh methane

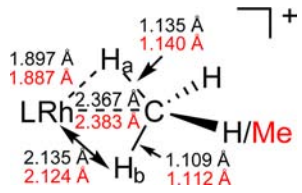

Figure 9. Structural parameters for the coordinated alkane ligand (methane in black and ethane in red) for the PONOP-trim ligand.

and ethane complexes with the PONOP-trim ligand. For the trimmed case, the methane and ethane ligands have nearly identical structural parameters. However, the rhodium is more electrophilic in the PONOP-trim complex, so the adjustment in the orientation of the alkane ligand is the net result of steric and electronic factors.

Selected bond distances for both the rhodium and iridium PONOP and PONOP-trim alkane complexes are reported in Table 1. Stronger binding of the alkane ligand to iridium can be inferred from the structural data in which the coordinated C−H bond is elongated by 0.03−0.04 Å relative to the Rh complex, and the M−H_a distance is ca. 0.1 Å shorter. It is interesting to note that the Ir−C distances for the rhodium and iridium complexes are nearly identical, while the M−H_b distances are more than 0.12 Å longer for the Ir complexes.

For the Rh and Ir PONOP-trim complexes, an axial agostic interaction is found in the energy minimum for the ethyl hydride oxidative cleavage product (see Figure 10b). However, this minimum lies only 1.5 kcal/mol lower in energy than the terminal ethyl conformer, $[(\text{PONOP-trim})\text{Ir}(\text{H})(\eta^2\text{-CH}_2\text{CH}_3)]^+$ (Figure 10a). The structural parameters in Table 1 and the energies in Table 2 are listed for the pictured terminal ethyl conformer. In contrast, for the full PONOP complexes the axial agostic minimum lies above the terminal ethyl ground state, presumably because of crowding of the axial site by the *t*Bu groups.

The energetics of the alkane dissociation (eq 1) and the oxidative cleavage reaction (eq 2) were examined for Rh and Ir

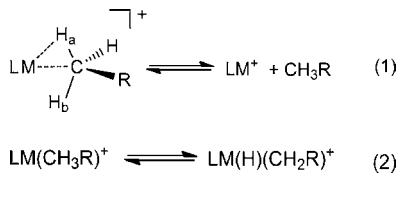

coordinated by the full PONOP and the PONOP-trim ligand. The data are summarized in Figure 11 and Table 2.

The most striking difference between the rhodium and iridium pincer alkane complexes is their relative positions on the energy surface with respect to the alkyl hydride oxidative cleavage product. For iridium, the ground state is the alkyl hydride oxidative cleavage product, and the alkane complex is an intermediate along the alkane dissociation coordinate, while for rhodium, the alkane complex is the ground state. The enthalpy and free energy for alkane loss (eq 1) is more positive for the PONOP-trim complexes than for the PONOP complexes, and for each ligand/alkane pair, the iridium complex binds the alkane more strongly by ∼5 kcal/mol than for Rh (Figure 11). There is a change in the relative binding

dx.doi.org/10.1021/ja4079539 | J. Am. Chem. Soc. 2013, 135, 15933−15947

Table 1. Structural Parameter for Cationic (PONOP)M and (PONOP-trim)M Alkane and Alkyl Hydride Complexes[a,b]

complex	C−H$_a$	C−H$_b$	M−H$_a$[c]	M−H$_b$	M−C	M−N	M−P
[(PONOP)Rh(CH$_4$)]$^+$	1.137	1.105	1.869	2.177	2.380	2.016	2.290
[(PONOP-trim)Rh(CH$_4$)]$^+$	1.135	1.109	1.897	2.135	2.367	2.012	2.263
[(PONOP)Ir(CH$_4$)]$^+$	1.172	1.098	1.782	2.300	2.365	2.011	2.290
[(PONOP-trim)Ir(CH$_4$)]$^+$	1.171	1.100	1.797	2.282	2.359	2.009	2.266
[(PONOP)Rh(CH$_3$Me)]$^+$	1.144	1.105	1.863	2.239	2.431	2.019	2.295
[(PONOP-trim)Rh(CH$_3$Me)]$^+$	1.140	1.112	1.887	2.124	2.383	2.014	2.264
[(PONOP)Ir(CH$_3$Me)]$^+$	1.178	1.098	1.777	2.376	2.422	2.013	2.294
[(PONOP-trim)Ir(CH$_3$Me)]$^+$	1.179	1.102	1.782	2.286	2.382	2.012	2.267
[(PONOP)Rh(H)(CH$_3$)]$^+$			1.496		2.058	2.107	2.297
[(PONOP-trim)Rh(H)(CH$_3$)]$^+$			1.498		2.049	2.104	2.275
[(PONOP)Ir(H)(CH$_3$)]$^+$			1.526		2.083	2.112	2.301
[(PONOP-trim)Ir(H)(CH$_3$)]$^+$			1.528		2.071	2.114	2.281
[(PONOP)Rh(H)(CH$_2$Me)]$^+$			1.498		2.077	2.130	2.311
[(PONOP-trim)Rh(H)(CH$_2$Me)]$^+$			1.504		2.054	2.116	2.275
[(PONOP)Ir(H)(CH$_2$Me)]$^+$			1.525		2.100	2.132	2.310
[(PONOP-trim)Ir(H)(CH$_2$Me)]$^+$			1.531		2.077	2.124	2.281

[a]Bond distances given in Å. [b]Numbering scheme as in Figure 9. [c]The M−H distance for the alkyl hydride complexes.

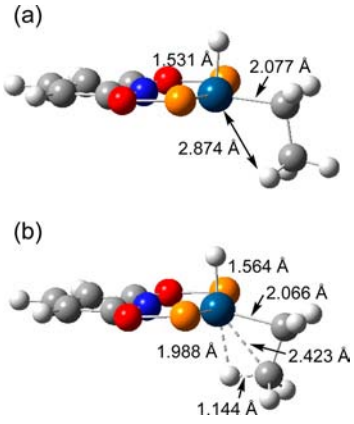

Figure 10. Structural diagram and bonding distances for (a) [(PONOP-trim)Ir(H)(CH$_2$CH$_3$)]$^+$ and (b) the axial agostic complex, [(PONOP-trim)Ir(H)(η^2-CH$_2$CH$_3$)]$^+$.

preference of methane and ethane associated with the change in the PONOP ligand. For both Rh and Ir PONOP-trim complexes, ethane is bound more strongly than methane, while for the PONOP complexes, the ethane ligand is more weakly bound than methane. The interaction of the more bulky ethane ligand with the ligand substituents appears to be the origin of the change in relative binding preference.

A primary purpose of the computational study was to gain insight into the mechanism of the exchange processes observed by dynamic NMR spectroscopy. For the calculation of the reaction barriers, the PONOP-trim ligand system was employed, which highlights the influence of the electronic preferences of the metal on the studied transformations. Shown in Figure 12 is the calculated free energy profile for reaction of the 14-electron [(PONOP-trim)M]$^+$ complexes with methane. The energy of **TS1** is not directly obtained from the calculations. For dissociation of a neutral ligand from a transition-metal complex that does not rearrange following dissociation (like the complexes herein), assuming the recoordination of the alkane is enthalpically barrierless, the alkane dissociation enthalpy (ΔH°) is an upper limit to the $\Delta G^\ddagger$ for methane dissociation (Figure 13). The actual $\Delta G^\ddagger$ for methane release will be determined by the degree to which the favorable entropy of alkane dissociation is reflected in the transition state.[74] For the inclusion of this transition state in the reaction coordinate diagram, ΔH° for the reaction is used, and thus **TS1** values in Figure 12 represent maximum values. For [(PONOP-trim)Ir(Me)(H)]$^+$, the barrier for methane loss is referenced to the methyl hydride ground state, which affords additional stability for the iridium complex to methane loss beyond the ~5 kcal/mol stronger binding of methane to Ir in comparison to Rh (Figure 12, left).

The experimental barrier for exchange between the hydride and the methyl signals for [(PONOP)Ir(Me)(H)]$^+$ (9.6 kcal/mol at −105 °C), corresponds to the barrier for reductive coupling of methyl and H to form the methane complex (Figure 12, left, **3-Ir→2-Ir**). Even though the ground state of the methane complex involves coordination of a single C−H bond, there are

Table 2. Calculated Enthalpy, Entropy, and Free Energies of Oxidative Cleavage and Alkane Dissociation at 298 K[a,b]

	PONOP-trim ligand						PONOP ligand					
	methane			ethane			methane			ethane		
	ΔH°	ΔS°	ΔG°	ΔH°	ΔS°	ΔG°	ΔH°	ΔS°	ΔG°	ΔH°	ΔS°	ΔG°
Oxidative Cleavage (eq 2)												
Ir	−4.9	−1.4	−5.1	−4.0	−0.6	−3.9	−7.6	−0.2	−7.5	−5.9	−0.8	−5.6
Rh	8.9	−1.6	9.4	8.5	−2.3	9.2	6.2	−1.5	6.6	7.6	−2.3	8.3
Alkane Dissociation (eq 1)												
Ir	22.1	33	12.1	23.3	35	12.9	19.5	34	9.4	18.6	38	7.3
Rh	17.4	31	8.1	18.4	34	8.4	15.0	33	5.2	14.1	37	3.0

[a]Enthalpies and free energies in kcal/mol and entropy in cal/mol·K. [b]Free energies at 298 K.

dx.doi.org/10.1021/ja4079539 | J. Am. Chem. Soc. 2013, 135, 15933−15947

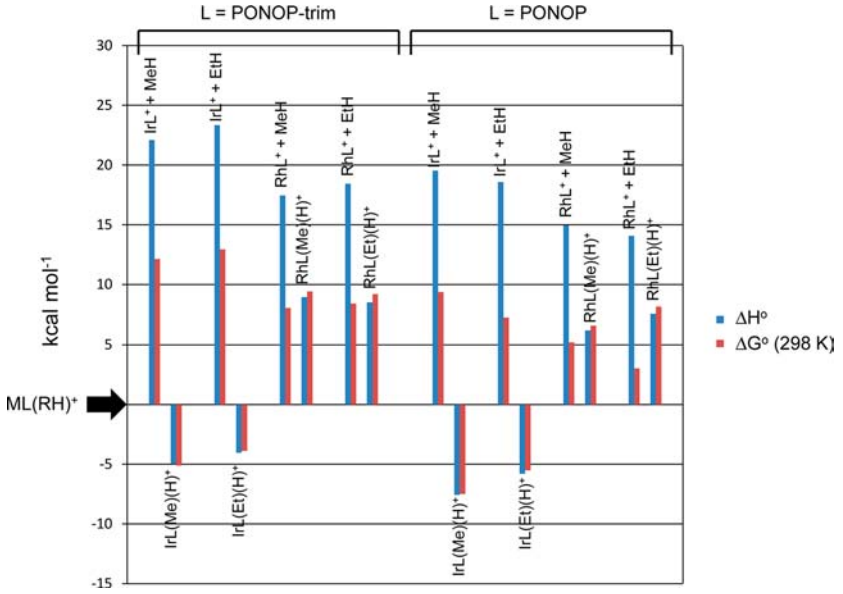

Figure 11. Calculated reaction enthalpies and free energies (kcal/mol) for Rh and Ir pincer complexes relative to the alkane complex, $[(PONOP)M(CH_3R)]^+$ (R = Me, H) at 298 K. Enthalpies and free energies are reported relative to the alkane complexes.

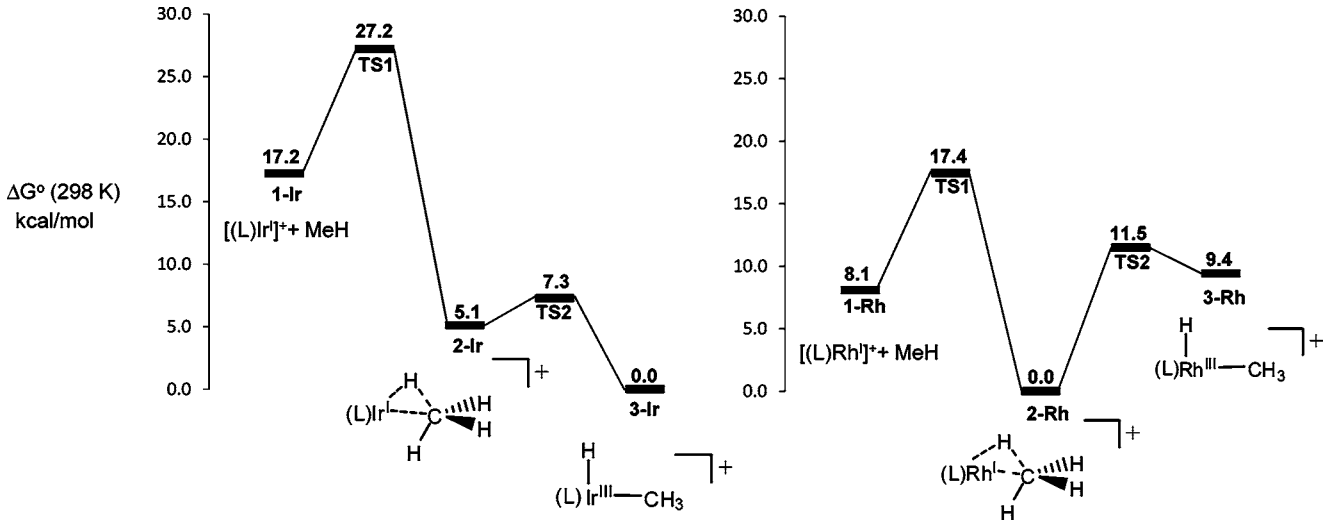

Figure 12. Calculated free energy profile (kcal/mol) for methane addition to the 14-electron Rh and Ir pincer complexes, $[(PONOP\text{-}trim)M]^+$ at 298 K. Enthalpies and free energies are reported relative to the methane complex for the case of Rh and to the methyl hydride complex for the case of Ir. **TS1** was estimated by the ΔH° for methane loss reaction and represents a maximum value (see text).

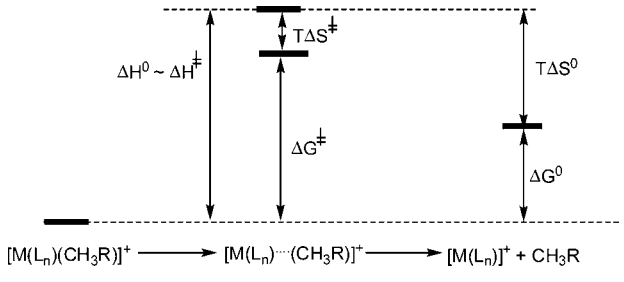

Figure 13. Reaction coordinate diagram for alkane dissociation.

low barrier processes to equilibrate all of the hydrogens in the methane ligand, including a rocking motion (eq 3), which is essentially flat on the potential energy surface, and rotation about the coordinated C−H bond (eq 4), which has a barrier less than 2.5 kcal/mol for Ir. Both of these processes need to be operative to equilibrate all of the hydrogen positions. These low

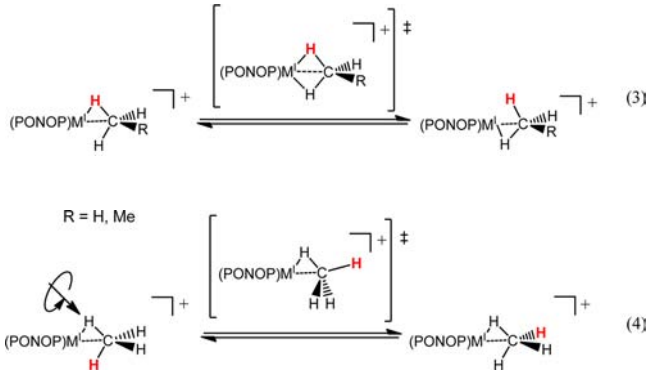

barriers support the notion that once the iridium methane complex is formed, all of the hydrogens rapidly interchange, and are also consistent with the fact that only a single proton

dx.doi.org/10.1021/ja4079539 | J. Am. Chem. Soc. 2013, 135, 15933−15947

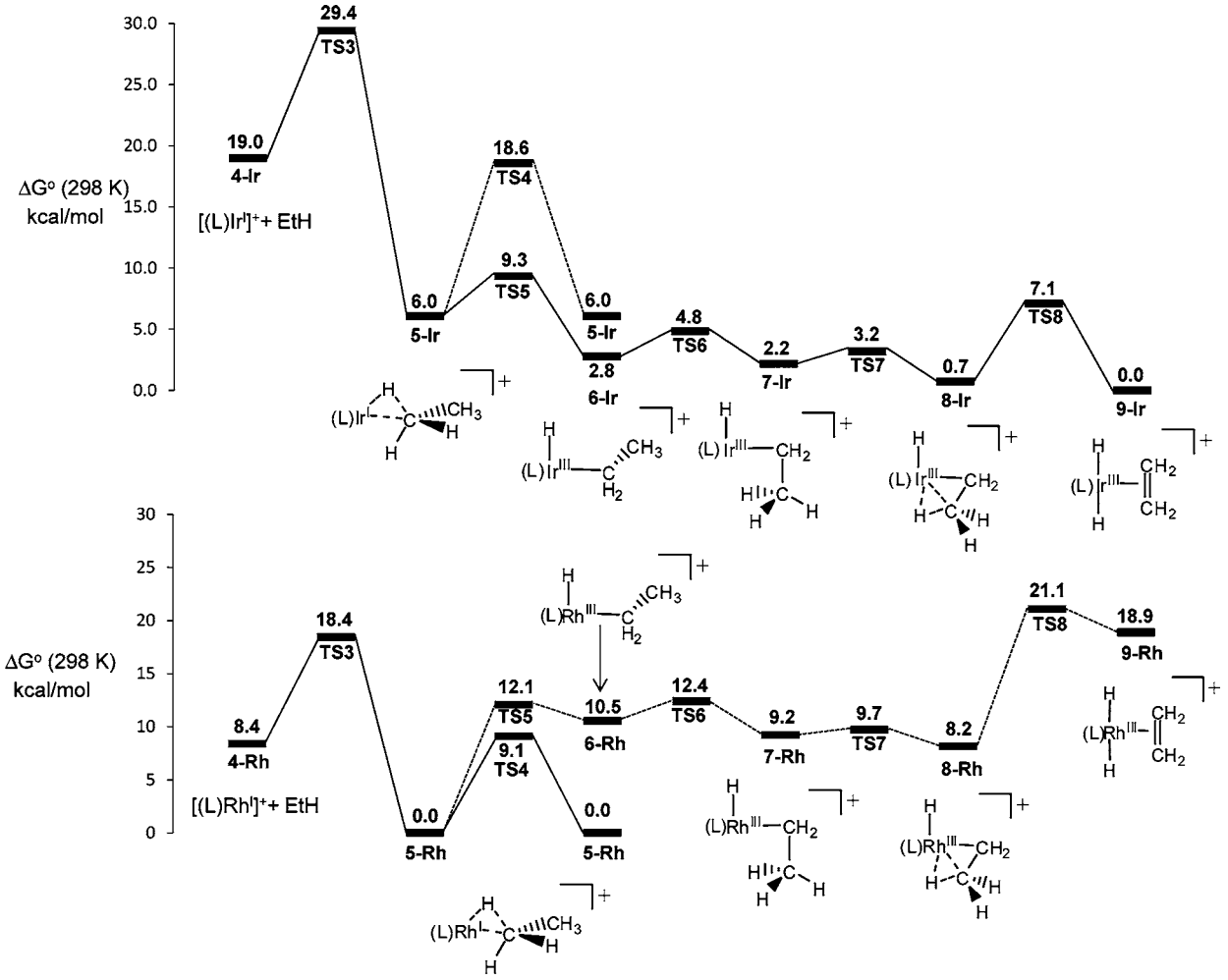

Figure 14. Calculated free energy profile (kcal/mol) for ethane addition to the 14-electron Rh and Ir Pincer complexes, $[(PONOP\text{-}trim)M]^+$ at 298 K. Free energies are reported relative to the methane complex for Rh and to the ethylene dihydride complex for Ir. As for the methane complexes, **TS3** was estimated by the ΔH° for the ethane loss reaction and represents a maximum value (see text).

resonance is observed for the four hydrogens in the coordinated methane ligand in **2-(MeH)**$^+$, even at −140 °C.[58]

The free energy profiles for reaction of the 14-electron $[(PONOP\text{-}trim)M]^+$ complexes with ethane are shown in Figure 14. The first steps of the reactions to produce the ethyl hydride complexes closely resemble the methane case. For the ethane complexes, the dynamic NMR studies reported above allowed determination of a barrier for chain-walking (interchange of C_α and C_β), which requires interaction of the metal center with the unbound methyl group in the alkane complex, $[(PONOP\text{-}trim)M(\sigma\text{-}C_2H_6)]^+$, or the alkyl hydride, $[(PONOP\text{-}trim)M(Et)(H)]^+$. For rhodium (Figure 14 bottom), chain-walking from the σ-ethane ground state, **5-Rh**, would occur via the η^2-ethane transition, **TS4**, graphically depicted in eq 5 and

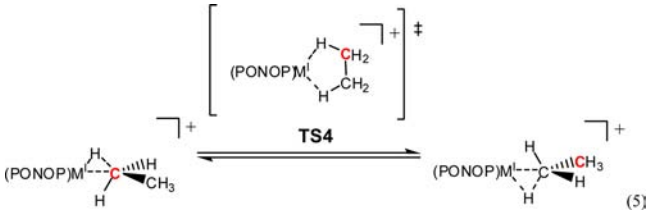

Figure 15. The ethane ligand remains staggered in the transition state, forcing a twist of the ethane ligand relative to

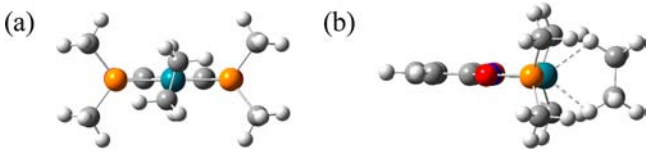

Figure 15. Two views of the η^2-ethane transition state that equilibrates C_α and C_β for Rh (**TS4** in Figure 14).The H−Rh distances are 2.138 Å and the corresponding C···H distances are 1.117 Å.

the normal of the pincer plane passing through N to maintain effective coordination of the two C−H bonds (Figure 15, left).

The alternate pathway explored for chain-walking proceeds through the ethyl hydride complex, **6-Rh**, which lies 11 kcal/mol higher in energy than **5-Rh**. The initial conformation of the ethyl hydride (**6-Rh** in Figure 14, bottom) has the methyl group in the same orientation as the methyl group of the ethane ligand. Rotation by 90° about the Rh−C bond places the methyl group in close proximity to the metal (**7-Rh**). The very low barrier for the formation of the axial agostic complex, **8-Rh**, is associated with rotation about the C−C bond in **7-Rh** to orient the hydrogen in an appropriate position to coordinate in the axial position. β-Hydride elimination from **8-Rh** to form $[(PONOP\text{-}trim)Rh(C_2H_4)(H)_2]^+$ (**9-Rh**) has a barrier of 13 kcal/mol. Complex **9-Rh** has a plane of symmetry through the

dx.doi.org/10.1021/ja4079539 | J. Am. Chem. Soc. 2013, 135, 15933−15947

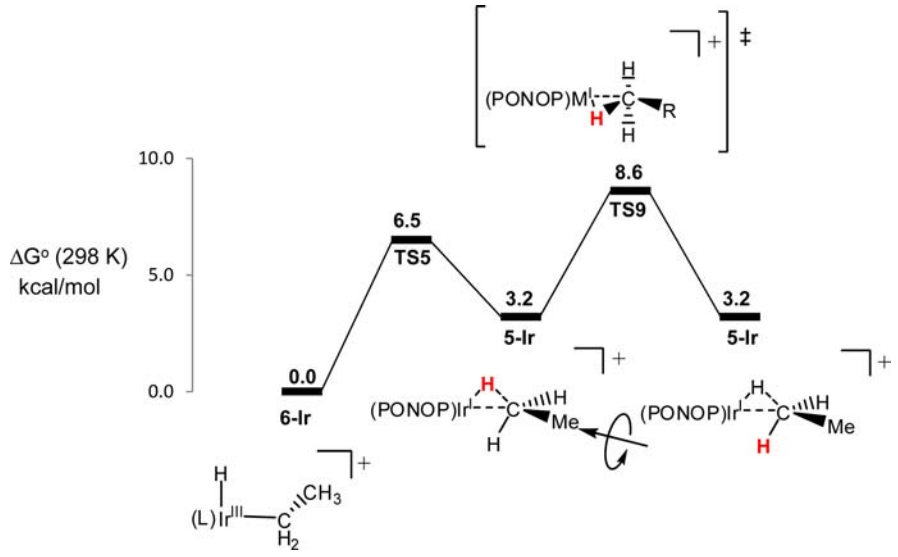

Figure 16. Calculated free energy profile (kcal/mol) for α-CH_2 hydride scrambling in **6-Ir** showing the barrier for in-place rotation for the σ-ethane complex, **5-Ir**, referenced to the alkyl hydride, **6-Ir**.

pincer ligand that inter-relates the two ethylene carbons, meeting the requirements for exchange. The overall barrier for the C_α–C_β exchange from **5-Rh** proceeding through **TS5** is ~21 kcal/mol. The lowest energy chain-walking pathway for rhodium proceeds through the ethane complex ground state via **TS4**, with a calculated barrier of 9 kcal/mol. For iridium (Figure 14, top), interchange via the η^2-ethane transition state (**TS4**), incurs an energetic penalty of ~3 kcal/mol to form the σ-ethane complex, **5-Ir**, from the ethyl hydride (**6-Ir**). Moreover, for Ir, **TS4** represents the high point on the energy profile and lies 13 kcal/mol above **5-Ir**. The calculated chain-walking barrier in the iridium ethane complex, **5-Ir**, of 12.6 kcal/mol is 3.5 kcal/mol higher than the corresponding barrier in **5-Rh** of 9.1 kcal/mol. However, the alternate chain-walking pathway that proceeds through [(PONOP-trim)Ir-$(C_2H_4)(H)_2$]$^+$ (**9-Ir**) is calculated to be the lowest energy pathway. This results not only from the lower relative energy of the ethyl hydride species **6-Ir** relative to the ethane complex **5-Ir**, but more importantly, from the similar energies for the axial agostic complex, **8-Ir**, the ethylene dihydride product, **9-Ir** and the low barrier connecting them.

For **1-(Et)(H)**$^+$, the barrier for scrambling the hydrogens on C_α with the hydride ligand is experimentally measurable and this exchange presumably proceeds through the σ-ethane complex. The requirement to fit the terminal methyl group in the σ-complex **1-(EtH)**$^+$ between the *t*Bu groups effectively shuts down the exchange via rotation about the coordinated C–H bond (eq 4), requiring an "in-place" rotation[75−78] to effect complete exchange of the α-hydrogens in **5-Ir** (Figure 16). This process is associated with a barrier of 5.4 kcal/mol for **5-Ir**, which is larger than the barrier for the oxidative cleavage of the C–H bond in the ethane complex (**5-Ir**→**TS5**), making **TS9** the high point. Accordingly, the experimental barrier for scrambling the C_α hydrogens measured for **1-(Et)(H)**$^+$, has a contribution from the energetic penalty to form the σ-ethane complex, **5-Ir**, from **6-Ir** and the barrier for in-place rotation (**5-Ir**→**TS9**). For rhodium, since the ground state is the σ-ethane complex, **5-Rh**, the barrier for in-place rotation will determine the rate for scrambling the C_α hydrogens. For **5-Rh**, this barrier is 4.7 kcal/mol, which is too low to be experimentally observable.

The comparison between the calculated energy profiles for the PONOP-trim ligand complexes to the experimental system has to be done with care, but several clear implications emerge from this DFT study: (1) For rhodium, the most likely pathway for exchange of C_α and C_β proceeds through the η^2-ethane transition state, **TS4**. The high position of the ethylene dihydride complex, **9-Rh**, on the energy surface (+19 kcal/mol) makes it unlikely that exchange via this pathway would be accessed prior to ethane dissociation. (2) For iridium, the experimental barriers for Ir–H/α-CH_2 exchange and C_α–C_β exchange are very similar (7.2 and 8.1 kcal/mol, respectively, at −110 °C). If both processes proceed through the σ-ethane complex, **5-Ir**, this would imply that the barrier for in-place rotation (**TS9**, Figure 16) is only 1 kcal/mol less than the barrier for exchange via the η^2-ethane transition state (**TS4**), which seems highly unlikely given the barriers calculated for the (PONOP-trim)Ir complexes. Alternatively, the ethyl hydride, **6-Ir**, the axial agostic, **8-Ir**, and the ethylene dihydride, **9-Ir**, are positioned within 3 kcal/mol on the energy surface, with the highest barrier of 7.1 kcal/mol separating **8-Ir** and **9-Ir**. Overall, the alternate pathway for C_α–C_β exchange via **9-Ir** is more compatible with the similar Ir–H/α-CH_2 and C_α–C_β barriers observed experimentally.

It is also desirable to compare the calculated barriers for alkane loss to the experimentally determined values. However, this requires that the temperature at which the experimental measurements were performed be taken into account, and an estimate of the entropic contribution to the free energy of activation for alkane loss needs to be made. Shown in Table 3 are computed barriers for alkane loss using the data for the (PONOP)M complexes. At the experimental temperature an entropic contribution to the free energy is calculated, and this number is weighted by a factor of 0.4, a value estimated in a methane dissociation study performed by Hall and co-workers.[74] For the iridium complexes, the free energy difference between the alkyl hydride ground state and the transition state needs to be included when calculating the free energy of activation.

dx.doi.org/10.1021/ja4079539 | J. Am. Chem. Soc. 2013, 135, 15933−15947

Table 3. Calculated Activation Free Energies for Alkane Loss[a]

	alkane loss reaction (eq 1)								
	ΔH^{o}	ΔS^{o}	T (K)[b]	$T\Delta S$	weighted $T\Delta S$[c]	$\Delta G^{\ddagger}$ (calc)	ΔG^{o} [d]	overall $\Delta G^{\ddagger}$ (calc)	$\Delta G^{\ddagger}$ (exp)
$Rh(PONOP)^{+}/CH_4$	15	33	186	6.1	2.5	12.5		12.5	14.5
$Rh(PONOP)^{+}/C_2H_6$	14.1	37	141	5.2	2.6	11.5		11.5	10.9
$Ir(PONOP)^{+}/CH_4$	19.5	34	295	10.0	4.0	15.5	7.6	23.1	22.4
$Ir(PONOP)^{+}/C_2H_6$	18.6	38	233	8.8	3.5	15.1	5.9	21.0	17.4

[a]Enthalpies and free energies in kcal/mol and entropy in cal/mol·K. [b]Temperature for experimental measure of $\Delta G^{\ddagger}$. [c]Estimate of entropy contribution to the transition state[74] is set at 40%. [d]Free energy difference between alkyl hydride and alkane cation.

A reasonable agreement between the calculated and experimental data is obtained from this approach.

SUMMARY AND IMPLICATIONS

Low-temperature protonation of (PONOP)Rh−CH_2CH_3, **2-Et**, leads to a σ-ethane complex, (PONOP)Rh$(CH_3CH_3)^{+}$, **2-(EtH)**$^{+}$, characterized by ^{1}H and ^{13}C NMR spectroscopy at −143 °C. NMR data show that ethane is bound to one methyl group and DFT computations suggest, in analogy with the previously observed methane complex, (PONOP)Rh$(CH_4)^{+}$, **2-(MeH)**$^{+}$, that binding occurs primarily via a 3c,2e-interaction with one C−H bond. The barrier to site exchange among the three C−H bonds of the bound methyl group is too low to be determined by low-temperature NMR spectroscopy, consistent with the DFT predicted barrier of 4.7 kcal/mol. Dynamic NMR studies establish a barrier for migration of Rh from one methyl group to the other of 7.2(1) kcal/mol (−132 °C). Loss of ethane occurs with a barrier of 10.9(2) kcal/mol (−132 °C), considerably lower than the loss of methane from **2-(MeH)**$^{+}$ (14.5 kcal/mol, −87 °C) because of increased steric crowding in **2-(EtH)**$^{+}$.

It is instructive to compare the barrier to chain migration in **2-(EtH)**$^{+}$ to the analogous barriers in other systems. As noted earlier, deuterium labeling studies provide evidence that in rhodium alkyl hydride complexes studied by Jones[61] and Flood,[62] the σ-alkane complex intermediates formed upon reductive coupling exhibit rhodium migration along the alkane chain prior to alkane dissociation. However, the rates of this migration cannot be determined from these experiments. Based on ROESY experiments, Ball[45] has estimated that the rate constants for interconversion of the three nearly equally populated (i-PrC_5H_4)Re$(CO)_2$(pentane) isomers are ∼1−10 s^{-1} at −100 °C ($\Delta G^{\ddagger}$ ∼ 10 kcal/mol). Similarly, SST experiments suggest that end-to-end migration of (C_6Et_6)W(CO_3)(pentane) occurs with a barrier of ∼9 kcal/mol (−120 °C).[53] The barrier measured for **2-(EtH)**$^{+}$ is somewhat lower (∼7 kcal/mol). While numerous factors come into play in determining such barriers, a significant difference in the two sets of systems is that previously studied Re, Mn, and W alkane complexes are all 18-electron species, while the Rh complex studied here is a 16-electron species and the transition state for migration involves coordination of two C−H bonds (see structure **TS4**) which can be accommodated by the 14-electron (PONOP)Rh^{+} fragment.

Protonation of the third-row congener, (PONOP)Ir−CH_2CH_3, **1-Et**, leads to the ethyl hydride complex, (PONOP)-Ir(H)$(CH_2CH_3)^{+}$, **1-(H)(Et)**$^{+}$, which was characterized by ^{1}H and ^{13}C NMR spectroscopy at −143 °C. Site exchange of the Ir−H and Ir−CH_2− protons occurs with barrier of 7.2 kcal/mol via an ethane complex intermediate, consistent with the observation of exchange of −CH_3 and Ir−H protons ($\Delta G^{\ddagger}$ = 9.3 kcal/mol) in the methyl hydride analog, **1-(H)(CH$_3$)**$^{+}$. The barrier to ethane loss is 17.4 kcal/mol, lower than loss of methane from **1-(H)(CH$_3$)**$^{+}$, ($\Delta G^{\ddagger}$ = 22.4 kcal/mol, 22 °C). End-to-end scrambling of the ethyl group (C_α−C_β site exchange) occurs with a barrier of 8.1(1) kcal/mol (−110 °C) as determined by dynamic ^{13}C NMR spectroscopy. While this scrambling process could be envisioned to occur via reductive coupling to the ethane intermediate, **1-(EtH)**$^{+}$, followed by chain-walking (in analogy with the Rh complex) and collapse back to **1-(H)(Et)**$^{+}$, DFT computations suggest this barrier is considerably higher than a process involving β-elimination to a symmetrical ethylene dihydride, **1-(H)$_2$(C$_2$H$_4$)**$^{+}$, followed by reinsertion. This mechanism is available for **1-(H)(Et)**$^{+}$ since this is a 16-electron complex and possesses a vacant coordination site. In contrast, the Rh alkyl hydride complexes examined by Jones and Flood are both 18-electron complexes and thus a β-elimination, readdition mechanism is unavailable for chain-walking in these complexes.

Investigations of the factors controlling the relative stabilities of transition-metal alkyl hydride vs transition-metal σ-alkane complexes, the kinetics of their interconversion, and the binding affinities and rates of interconversion of alkane complex isomers are ongoing in these laboratories. DFT calculations will provide effective screening of promising ligand/metal combinations. Such fundamental information regarding transition-metal/alkane interactions should prove useful in developing new systems for selective activation of unactivated C−H bonds.

EXPERIMENTAL SECTION

General Considerations. All reactions, unless otherwise stated, were conducted under an atmosphere of dry, oxygen free argon using standard high-vacuum, Schlenk, or drybox techniques. Argon was purified by passage through BASF R3-11 catalyst (Chemalog) and 4 Å molecular sieves. ^{1}H, ^{13}C{^{1}H}, ^{1}H−^{1}H COSY, ^{1}H−^{13}C HSQC, ^{1}H−^{1}H NOESY, and ^{13}C DEPT135 NMR spectra were recorded on a Bruker DRX 500 MHz, a Bruker DRX 400 MHz, or a Bruker 400 MHz AVANCE spectrometer. ^{1}H and ^{13}C chemical shifts are referenced relative to residual $CHCl_3$ (δ 7.24 for ^{1}H), $CH(D)Cl_2$ (δ 5.32 for ^{1}H), $CHCl_2F$ (δ 7.47 for ^{1}H), C_6HD_5 (δ 7.15 for ^{1}H), $^{13}CD_2Cl_2$ (δ53.8 for ^{13}C), $^{13}CDCl_3$ (δ77.0 for ^{13}C), $^{13}CDCl_2F$ (δ 104.2 for ^{13}C), and $^{13}C_6D_6$ (δ 128.0 for ^{13}C); ^{31}P chemical shifts are referenced to an external standard of H_3PO_4. Probe temperatures were calibrated using ethylene glycol and methanol as previously described.[79] Because of strong ^{31}P−^{31}P coupling in the pincer ligand, many ^{1}H and ^{13}C NMR signals appear as virtual triplets (vt) and are reported as such with the apparent coupling noted. The ^{1}H and ^{13}C{^{1}H} NMR spectral data for the B$(Ar_F)_4$ anion (B$(Ar_F)_4$ = B[3,5-$(CF_3)_2C_6H_3)]_4$) in CD_2Cl_2 is identical for all complexes and is therefore not repeated below. **B(Ar$_F$)$_4$**: ^{1}H NMR: δ 7.80 (s, 8H, o-Ar), 7.56 (s, 4H, p-Ar). ^{13}C{^{1}H} NMR: δ 162.2 (q, 37 Hz, $ipso$-Ar), 135.2 (o-Ar), 129.3 (q, 31 Hz, m-Ar), 125.0 (q, 273 Hz, CF_3), 117.9 (p-Ar). Elemental analyses were carried out by Robertson Microlit Laboratories of Madison, NJ. Crystallographic data were also deposited with the Cambridge Crystallographic Data Centre. Copies of the data (CCDC No. 902641 and 902642) can be obtained free of charge via

dx.doi.org/10.1021/ja4079539 | J. Am. Chem. Soc. 2013, 135, 15933−15947

http://www.ccdc.cam.ac.uk/data_request/cif, by e-mailing data_request@ccdc.cam.ac.uk, or by contacting The Cambridge Crystallographic Data Centre, 12, Union Road, Cambridge CB 1EZ, U.K. (fax +44 1223 336033).

Materials. All solvents were deoxygenated and dried by passage over columns of activated alumina.[80,81] CD_2Cl_2, purchased from Cambridge Laboratories, Inc., was dried over CaH_2, vacuum transferred to a Teflon sealable Schlenk flask containing 4 Å molecular sieves, and degassed via three freeze−pump−thaw cycles. Freon ($CDCl_2F$) was prepared according to a literature procedure and stored over activated 4 Å molecular sieves at −25 °C.[82] $IrCl_3$ and $RhCl_3$ were purchased from J&J Materials or obtained from W.C. Heraeus GmbH and used as received. (PONOP)MCl (M = Ir[57] and Rh,[58] $[H(OEt_2)_2][B(Ar_F)_4]$[83] and MgR_2 (R = Et, Pr)[84] were synthesized according to literature methods. All other reagents were purchased from Aldrich, Acros, Alpha Aesar, or Strem Chemicals and used as received.

Preparation of (PONOP)Ir(C_2H_5) (1-Et). Under an argon atmosphere a Schlenk flask was charged with **1-IrCl** (0.168 g, 0.30 mmol) and $Mg(C_2H_5)_2$ (0.068 g, 0.85 mmol) and toluene solvent (∼7 mL). The reaction mixture was heated to 90 °C for 1 d. Volatiles were removed under dynamic vacuum and the red-brown residue was extracted into pentane. The brown-red pentane extracts were concentrated and cooled to −35 °C. After two days, red-brown crystals of **1-Et** formed. Yield: 0.075 g (0.12 mmol, 40%). ^{1}H NMR (C_6D_6, RT): δ 7.37 (t, 1H, $^3J_{HH}$ = 8.3 Hz, *p*-C_6H_3N), 6.10 (d, 2H, $^3J_{HH}$= 7.9 Hz, *m*-C_6H_3N), 2.78 (qt, 2H, $^3J_{HH}$ = 7.7 Hz, $^3J_{P-H}$ = 4.5 Hz, $IrCH_2CH_3$), 1.99 (t, 3H, $^3J_{HH}$ = 7.7 Hz, $IrCH_2CH_3$), 1.42 (vt, 36 H, J_{P-H} = 6.8 Hz, $C(CH_3)_3$). ^{31}P{^{1}H} NMR (C_6D_6, RT): δ 185.6 (s). ^{13}C{^{1}H} NMR (C_6D_6, RT): δ 163.0 (t, $^2J_{P-C}$ = 3.9 Hz, C_6H_3N), 131.0, 101.0 (t, $^3J_{P-C}$ = 2.3 Hz, C_6H_3N), 40.7 (vt, *J* = 7.4 Hz, P-$C(CH_3)_3$), 28.0 (vt, *J* = 4.0 Hz, P-$C(CH_3)_3$), 25.6 ($IrCH_2CH_3$), −13.2 (t, $^2J_{P-C}$ = 5.6 Hz, $IrCH_2CH_3$). Anal. calcd for $C_{23}H_{44}NO_2P_2Ir$: C, 44.50; H, 7.14; N, 2.25. Found: C, 44.35; H, 7.19; N, 2.30.

Preparation of (PONOP)Ir(C_3H_7) (1-Pr). Under an argon atmosphere a Schlenk flask was charged with **1-Cl** (0.155 g, 0.27 mmol) and $Mg(C_3H_7)_2$ (0.052 g, 0.47 mmol) and ∼5 mL of THF/toluene solvent (1:10). The reaction mixture was heated to 95 °C for 2 d. Volatiles were removed under dynamic vacuum, and the red brown residue was extracted into pentane. The brown-red pentane extracts were concentrated and cooled to −35 °C. After two days, purple crystals of **1-Et** formed. Yield: 0.053 g (0.083 mmol, 31%). ^{1}H NMR (C_6D_6, RT): δ 7.37 (t, 1H, $^3J_{HH}$ = 7.7 Hz, *p*-C_6H_3N), 6.10 (d, 2H, $^3J_{HH}$= 7.9 Hz, *m*-C_6H_3N), 2.73 ("m", 2H, $^3J_{HH}$ = 7.5 Hz, $^3J_{P-H}$ = 4.5 Hz, $IrCH_2CH_2CH_3$), 2.05 ("m", 2H, $IrCH_2CH_2CH_3$), 1.41 (vt, 36 H, J_{P-H} = 6.8 Hz, $C(CH_3)_3$), 1.42 (overlapped, 3H, $IrCH_2CH_2CH_3$). ^{31}P{^{1}H} NMR (C_6D_6): δ 186.1 (s). ^{13}C{^{1}H} NMR (C_6D_6): δ 163.3 (t, $^2J_{P-C}$ = 3.7 Hz, C_6H_3N), 131.1, 101.2 (t, $^3J_{P-C}$ = 2.4 Hz, C_6H_3N), 40.7 (vt, *J* = 8.4 Hz, P-$C(CH_3)_3$), 35.0 (t, $^4J_{P-C}$ = 2.1 Hz, $IrCH_2CH_2CH_3$), 28.1 (vt, *J* = 4.1 Hz, P-$C(CH_3)_3$), 22.5 ($IrCH_2CH_2CH_3$), 0.4 (t, $^2J_{P-C}$ = 5.9 Hz, $IrCH_2CH_2CH_3$). Anal. calcd for $C_{24}H_{46}NO_2P_2Ir$: C, 45.41; H, 7.30; N, 2.21. Found: C, 45.35; H, 7.37; N, 2.15.

The ^{2}H-labeled derivative (PONOP)Ir($CH_2CH_2CD_3$) was prepared analogous to **1-Pr** using **1-Cl** and $Mg(CH_2CH_2CD_3)_2$. Yield: 25%. ^{1}H NMR (C_6D_6, RT): δ 7.38 (t, 1H, $^3J_{HH}$ = 8.0 Hz, *p*-C_6H_3N), 6.10 (d, 2H, $^3J_{HH}$= 7.9 Hz, *m*-C_6H_3N), 2.72 ("m", 2H, $IrCH_2CH_2CD_3$), 2.02 ("m", 2H, $IrCH_2CH_2CD_3$), 1.41 (vt, 36 H, J_{P-H} = 6.8 Hz, $C(CH_3)_3$). ^{31}P{^{1}H} NMR (C_6D_6): δ 186.2 (s). ^{13}C{^{1}H} NMR (C_6D_6): δ 163.3 (t, $^2J_{P-C}$ = 3.8 Hz, C_6H_3N), 131.1, 101.2 (t, $^3J_{P-C}$ = 2.3 Hz, C_6H_3N), 40.7 (vt, *J* = 8.6 Hz, P-$C(CH_3)_3$), 34.9 (t, $^4J_{P-C}$ = 2.2 Hz, $IrCH_2CH_2CD_3$), 28.1 (vt, *J* = 3.9 Hz, P-$C(CH_3)_3$), 22.8 (sept, $IrCH_2CH_2CD_3$), +0.3 (t, $^2J_{P-C}$ = 6.0 Hz, $IrCH_2CH_2CD_3$).

Preparation of (PONOP)Rh(C_2H_5) (2-Et). Under an argon atmosphere a heavy-walled glass reaction vessel was charged with **2-Cl** (0.157 g, 0.33 mmol) and $Mg(C_2H_5)_2$ (0.030 g, 0.36 mmol) and ∼5 mL of THF/toluene solvent (10:1). The reaction mixture was allowed to stir at ambient temperature for 2 d. Volatiles were removed from the bright-red solution affording a red powder. The residue was extracted with pentane, filtered, concentrated, and the solution stored at −35 °C. Large red cubes formed within a few days. Yield: 0.102 g (0.192 mmol, 58%). ^{1}H NMR (C_6D_6, RT): δ 6.86 (t, 1H, $^3J_{HH}$ = 8.0 Hz, *p*-C_6H_3N), 6.16 (d, 2H, $^3J_{HH}$ = 8.0 Hz, *m*-C_6H_3N), 1.77−1.71 (m, 5H, CH_2CH_3), 1.41 (vt, 36H, *J* = 6.6 Hz, $C(CH_3)_3$). ^{31}P{^{1}H} NMR (C_6D_6, RT): δ 197.6 (d, $^1J_{Rh-P}$ = 185 Hz). ^{13}C{^{1}H} NMR (C_6D_6, RT): δ 163.0 (t, $^2J_{P-C}$ = 4.4 Hz, C_6H_3N), 134.8, 100.4 (t, $^3J_{P-C}$ = 2.0 Hz, C_6H_3N), 39.8 ("dd", *J* = 3.7 Hz, $^2J_{Rh-C}$ = 3.6 Hz, P-$C(CH_3)_3$), 28.3 (vt, *J* = 4.4 Hz, P-$C(CH_3)_3$), 22.8 (t, $^3J_{P-C}$ = 2.1 Hz, $IrCH_2CH_3$), −9.0 (dt, $^1J_{Rh-C}$ = 25.7 Hz, $^2J_{P-C}$ = 9.7 Hz, $IrCH_2CH_3$). Anal. calcd for $C_{23}H_{44}NO_2P_2Rh$: C, 51.98; H, 8.34; N, 2.64. Found: C, 52.05; H, 8.45; N, 2.58.

Generation of (PONOP)IrH (1-H). A J. Young NMR tube was charged with **1-Et** (15 mg) and 500 μL of C_7D_8, and the NMR tube was heated at 135 °C. The β-hydride elimination was monitored by ^{31}P NMR spectroscopy over ∼2 half-lives. The decay of the resonance for **1-Et** was converted to a concentration and fitted to first-order plots of ln[**1-Et**] vs time which gave observed rate constants as the slope (see SI for details). Complex **1-Et** was cleanly converted to **1-H** and C_2H_4. NMR data of **1-H**: ^{1}H NMR (C_7D_8, RT): δ 7.43 (t, 1H, $^3J_{HH}$ = 8.0 Hz, *p*-C_6H_3N), 6.17 (d, 2H, $^3J_{HH}$ = 8.0 Hz, *m*-C_6H_3N), 1.41 (vt, 36H, *J* = 7.7 Hz, $C(CH_3)_3$), −6.87 (t, 1H, $^2J_{P-H}$ = 16.5 Hz, Ir−*H*). ^{31}P{^{1}H} NMR (C_7D_8, RT): δ 213.2.

Observation of [(PONOP)Ir(H)(C_2H_5)][$N(SO_2CF_3)_2$] (1-(H)(Et)$^+$). A screw cap NMR tube was charged with $HN(SO_2CF_3)_2$ (0.019 g, 0.068 mmol) and **1-Et** (0.017 g, 0.027 mmol). At 77 K ∼500 μL $CDCl_2F$ was transferred into the tube via a cannula. The NMR tube was transferred into a cooling bath which was precooled to −100 °C. After the sample thawed, the screw cap was removed, and the sample was mixed under a flow of argon with glass rod until a homogeneous solution formed. The NMR tube was capped again and cooled to 77 K. The sample was maintained at 77 K until inserted into the precooled NMR probe at −143 °C. After the sample thawed, **1-(H)(Et)**$^+$ was monitored by multinuclear NMR spectroscopy. A typical experiment yielded 100% conversion of **1-Et** to **1-(H)(Et)**$^+$, but care had to be observed since significant sample degradation was observed when the sample was allowed to warm above −40 °C. ^{1}H NMR ($CDCl_2F$, −143 °C): δ 7.92 (t, 1H, $^3J_{HH}$ = 8.2 Hz, *p*-C_6H_3N), 7.02 (d, 2H, $^3J_{HH}$ = 8.2 Hz, *m*-C_6H_3N), 2.65 (br.s., 2H, CH_2CH_3), 1.40 (br.s., CH_2CH_3 3H), 1.35 (br.s., 36H, $C(CH_3)_3$), −42.3 (t, 1H, $^2J_{P-H}$ = 13.5 Hz, Ir−*H*). ^{1}H NMR ($CDCl_2F$, −87 °C): δ 7.92 (t, 1H, $^3J_{HH}$ = 8.2 Hz, *p*-C_6H_3N), 7.03 (d, 1H, $^3J_{HH}$ = 8.2 Hz, *p*-C_6H_3N), 2.65 (br.s, 2H, CH_2CH_3), 1.40 (br.s., CH_2CH_3 3H), 1.35 (vt, 36H, *J* = 7.7 Hz, $C(CH_3)_3$), no Ir−*H* and Ir−CH_2CH_3 resonances detected. ^{31}P{^{1}H} NMR ($CDCl_2F$, −143 °C): δ 183.2. ^{13}C{^{1}H} NMR (C_6D_6, −143 °C): δ 161.8 (C_6H_3N), 144.2, 103.4, 42.9 (vt, *J* = 9.7 Hz, P-$C(CH_3)_3$), 40.4 (vt, *J* = 9.7 Hz, P-$C(CH_3)_3$), 26.3 (br.s., P-$C(CH_3)_3$), 21.5 ($IrCH_2CH_3$), −10.9 (br.t., coupling not resolved, $IrCH_2CH_3$).

Observation of [(PONOP)Ir(H)(C_3H_7)][$N(SO_2CF_3)_2$] (1-(H)(Pr)$^+$). A screw cap NMR tube was charged with $HN(SO_2CF_3)_2$ (0.018 g, 0.064 mmol) and **1-Pr** (0.017 g, 0.027 mmol). At 77 K ∼500 μL $CDCl_2F$ was transferred into the tube via a cannula. The NMR tube was transferred into a cooling bath which was precooled to −100 °C. After the sample thawed, the screw cap was removed, and the sample was mixed under a flow of argon with glass rod until a homogeneous solution formed. The NMR tube was capped again and cooled to 77 K. The sample was maintained at 77 K until inserted into the precooled NMR probe at −143 °C. After the sample thawed, **1-(H)(Pr)**$^+$ was monitored by multinuclear NMR spectroscopy. A typical experiment yielded 100% conversion of **1-IrPr** to **1-(H)(Pr)**$^+$, but care had to be observed since significant sample degradation was observed when the sample was allowed to warm above −40 °C. ^{1}H NMR ($CDCl_2F$, −143 °C): δ 7.92 (t, 1H, $^3J_{HH}$ = 8.4 Hz, *p*-C_6H_3N), 7.02 (d, 2H, $^3J_{HH}$ = 8.4 Hz, *m*C_6H_3N), 2.56 (br.s., 2H, $CH_2CH_2CH_3$), 1.55 (br.s., $CH_2CH_2CH_3$, 2H), 1.33 (br.s., 36H, $C(CH_3)_3$), −42.3 (t, 1H, $^2J_{P-H}$ = 13.3 Hz, Ir−*H*). ^{31}P{^{1}H} NMR ($CDCl_2F$, −143 °C): δ 183.5. ^{13}C{^{1}H} NMR (C_6D_6, −143 °C): δ 161.8 (C_6H_3N), 144.2, 103.4, 42.9 (vt, *J* = 10.2 Hz, P-$C(CH_3)_3$), 40.4 (vt, *J* = 10.2 Hz, P-$C(CH_3)_3$), 26.4 (br.s., P-$C(CH_3)_3$), 30.8 ($^1J_{CH}$ = 121 Hz, $IrCH_2CH_2CH_3$), 19.8 ($^1J_{CH}$ = 127 Hz, $IrCH_2CH_2CH_3$), −1.05 ($^1J_{CH}$ = 121 Hz, $^2J_{P-H}$ coupling not resolved, $IrCH_2CH_2CH_3$).

dx.doi.org/10.1021/ja4079539 | J. Am. Chem. Soc. 2013, 135, 15933−15947

Observation of [(PONOP)Rh(C_2H_6)][B(Ar_F)$_4$] (2-(EtH)$^+$). A screw cap NMR tube was charged with [H(OEt_2)$_2$][B(Ar_F)$_4$] (0.032 g, 0.032 mmol), while another screw cap NMR tube was charged with **2-Et** (0.016 g, 0.030 mmol) and ~100 μL CD_2Cl_2. At 77 K ~300 μL $CDCl_2F$ was transferred into both NMR tubes. Since **2-Et** was only moderately soluble in pure $CDCl_2F$ the sample was thoroughly mixed at −90 °C to ensure that **2-Et** was completely dissolved before it was added via cannula transfer (−90 °C) to the second NMR tube which was kept at 77 K during the transfer process. The sample was maintained at 77 K until inserted into the precooled NMR probe at −143 °C. After the sample thawed, **2-(EtH)**$^+$ was monitored by multinuclear NMR spectroscopy. A typical experiment yielded a 2:1 ratio of the σ-ethane complex and the ethane loss product, although ratios of 6:1 were observed in samples where *extreme* caution was used to prevent warming of the NMR tube during sample preparation and manipulation. *Inattention to detail can cause complete loss of the σ-ethane complex within seconds.* ^{1}H NMR ($CDCl_2F/CD_2Cl_2$, −143 °C): δ 7.62 (t, 1H, $^3J_{HH}$ = 7.4 Hz, *p*-C_6H_3N), 6.69 (d, 2H, $^3J_{HH}$ = 7.4 Hz, *m*-C_6H_3N), 1.35 (br.s., 36H, C(CH_3)$_3$), 1.13 (br.s., 3H, Ir(CH_3CH_3)), −0.83 (br.s., 3H, Ir(CH_3CH_3)). ^{31}P{^{1}H} NMR ($CDCl_2F/CD_2Cl_2$), −143 °C): δ 208.1 (d, $^1J_{Rh-P}$ = 134 Hz). ^{13}C{^{1}H} NMR ($CDCl_2F/CD_2Cl_2$, −143 °C): δ 164.9 (C_6H_3N), 141.9, 103.6, 40.3 (br.vt, *J* = 4.9 Hz, P-$C(CH_3)_3$), 26.9 (br.s., P-C(CH_3)$_3$), 11.7 ($^1J_{CH}$ = 127 Hz, Ir(CH_3CH_3)), −31.6 ($^1J_{CH}$ = 124 Hz, Ir(CH_3CH_3)). The σ-ethane fragment was also confirmed by ^{13}C-DEPT135 experiments.

General Procedure for the Determination of Kinetics of Ethane Loss from 2-(EtH)$^+$. In a screw-cap NMR tube a sample **2-(EtH)**$^+$ was generated using the above procedure in $CDCl_2F$. The sample was warmed to −132 °C, and reaction progress was monitored by ^{31}P NMR spectroscopy over ~2 half-lives. The decay of the resonance for **2-(EtH)**$^+$ was converted to concentration and fitted to an exponential first-order decay plot of [**2-(EtH)**$^+$] vs time, which gave observed rate constants as the slope. Sample graphs of the kinetic data can be found in the Supporting Information.

General Procedure for Kinetic Determination of Site Exchange in 1-(H)Et$^+$ and 1-(H)Pr$^+$. In a screw-cap NMR tube, a sample of iridium complex of known concentration was prepared using above-mentioned procedures in dry $CDCl_2F$ under an Ar atmosphere. The tube was inserted into a temperature-calibrated probe, and the line-broadening of the Ir−*H* resonance was investigated at VT by selectively decoupled ^{1}H{^{31}P} NMR experiments. The rate of chain-walking was evaluated by line-broadening at VTs of the corresponding ^{13}C{^{1}H} NMR resonances. Eyring plots are provided in SI.

Computational Details. All DFT calculations were performed by using the Gaussian 09 package.[85] The basis-set/functional selection was based on a prior study of methane binding[58] and consists of the built-in 6-31G** basis set for all nontransition-metal atoms, the Stuttgart-Dresden basis set-pseudorelativistic effective core potential combination for the transition metals[86,87] with a single f-type polarization function for Rh and Ir (exponent =1.062 (Rh); 0.685 (Ir)) and the functional PBE0, the hybrid variant of PBE that contains 25% Hartree−Fock exchange[88] for geometry optimizations. The PBE0 functional was found to yield results in better agreement with experimental data than the B3LYP functional in an Ir pincer system[89] and has been endorsed as one of the best performing functionals for late transition-metal systems.[90] A similar basis set combined with the PBE0 functional was used to calculate weak Rh···H−C interactions in another system[91] and in our recent study of methane binding energies.[59] Frequency calculations were carried out on all minimum structures, and the resulting frequencies all had positive values. The nonscaled vibrational frequencies formed the basis for the calculation of vibrational zero point corrections and the standard thermodynamic corrections for the conversion of electronic energies to enthalpies and free energies at 298.15 K and 1 atm. Transition states were optimized in the gas phase using the Synchronous Transit-Guided Quasi-Newton (STQN) method implemented in Gaussian. Frequency calculations yielded one imaginary frequency for all transition states, and IRC calculations were carried out to confirm that the transition state identified connected the correct minima.

■ ASSOCIATED CONTENT

Ⓢ Supporting Information

^{31}P{^{1}H} NMR chemical shifts of (PONOP)Ir/Rh complexes, decay kinetics, Eyring plots for the H- and C-exchange processes, crystallographic details, pictures of the cooling "device", list of energies, free energies in au, and Cartesian coordinates of all optimized structures and transition states calculated systems and a complete list of authors for the Gaussian 09 program in noted in ref 85. This information is available free of charge via the Internet at http://pubs.acs.org/.

■ AUTHOR INFORMATION

Corresponding Author

mbrookhart@unc.edu

Notes

The authors declare no competing financial interest.

■ ACKNOWLEDGMENTS

We thank the National Science Foundation (CHE-1010170) for support, the Alexander-von-Humboldt Foundation for a Feodor-Lynen-Fellowship (M.D.W.), and Dr. David L. Harris for his help with NMR spectroscopy. M.D.W. gratefully acknowledges the current financial support by the Deutsche Forschungsgemeinschaft (DFG) through the Emmy Noether program (WA 2513/2-1) and W.C. Heraeus GmbH for a generous gift of $IrCl_3$.

■ REFERENCES

(1) Crabtree, R. H. *Chem. Rev.* **2010**, *110*, 575.
(2) *Activation and Functionalization of C-H Bonds*; Goldberg, K. I.; Goldman, A. S., Eds.; American Chemical Society: Washingon, D.C., 2004.
(3) *Activation of Unreactive Bonds and Organic Synthesis*; Murai, S., Ed.; Springer: Berlin Heidelberg, 1999; Vol. 3.
(4) Caballero, A.; Despagnet-Ayoub, E.; Mar, D.-R. M.; Diaz-Rodriguez, A.; Gonzalez-Nunez, M. E.; Mello, R.; Munoz, B. K.; Ojo, W.-S.; Asensio, G.; Etienne, M.; Perez, P. J. *Science* **2011**, *332*, 835.
(5) Kudrik, E. V.; Afanasiev, P.; Alvarez, L. X.; Dubourdeaux, P.; Clemancey, M.; Latour, J.-M.; Blondin, G.; Bouchu, D.; Albrieux, F.; Nefedov, S. E.; Sorokin, A. B. *Nat. Chem.* **2012**, *4*, 1024.
(6) Afanasiev, P.; Kudrik, E. V.; Millet, J.-M. M.; Bouchu, D.; Sorokin, A. B. *Dalton Trans.* **2011**, *40*, 701.
(7) Sorokin, A. B.; Kudrik, E. V.; Bouchu, D. *Chem. Commun.* **2008**, 2562.
(8) Chan, S. I.; Yu, S. S. F. *Acc. Chem. Res.* **2008**, *41*, 969.
(9) Baik, M.-H.; Newcomb, M.; Friesner, R. A.; Lippard, S. J. *Chem Rev* **2003**, *103*, 2385.
(10) Reis, P. M.; Silva, J. A. L.; Palavra, A. F.; Frausto, d. S. J. J. R.; Kitamura, T.; Fujiwara, Y.; Pombeiro, A. J. L. *Angew. Chem., Int. Ed.* **2003**, *42*, 821.
(11) Crabtree, R. H. *Chem. Rev.* **1995**, *95*, 987.
(12) Jones, W. D. *Science* **2000**, *287*, 1942.
(13) Labinger, J. A.; Bercaw, J. E. *Nature* **2000**, *417*, 507.
(14) Raybov, A. D. *Chem. Rev.* **1990**, *90*, 403.
(15) Arndtsen, B. A.; Bergman, R. G.; Mobley, T. A.; Peterson, T. H. *Acc. Chem. Res.* **1995**, *28*, 154.
(16) Shilov, A. E.; Shul'pin, G. B. *Chem. Rev.* **1997**, *97*, 2879.
(17) Crabtree, R. H. *Chem. Rev.* **1985**, *85*, 245.
(18) Sen, A. *Acc. Chem. Res.* **1998**, *31*, 550.
(19) Wolf, E. E. *Methane Conversion by Oxidative Processes*; Van Nostrand Reinhold: New York, 1992.
(20) Albrecht, M.; van Koten, G. *Angew. Chem., Int. Ed.* **2001**, *40*, 3750.
(21) Labinger, J. A. *J. Mol. Catal. A: Chem.* **2004**, *220*, 27.

(22) Cavaliere, V. N.; Crestani, M. G.; Pinter, B.; Pink, M.; Chen, C.-H.; Baik, M.-H.; Mindiola, D. J. *J. Am. Chem. Soc.* **2011**, *133*, 10700.
(23) Dobereiner, G. E.; Crabtree, R. H. *Chem. Rev.* **2010**, *110*, 681.
(24) Gol'dshleger, N. F.; Es'kova, V. V.; Shilov, A. E.; Shteinman, A. A. *Zh. Fiz. Khim.* **1972**, *46*, 1353.
(25) Periana, R. A.; Taube, D. J.; Gamble, S.; Taube, H.; Satoh, T.; Fujii, H. *Science* **1998**, *280*, 560.
(26) Periana, R. A. M., O.; Taube, D. J.; Bhalla, G.; Jones, C. J. *Science* **2003**, *301*, 814.
(27) Shilov, A. E. *Pure Appl. Chem.* **1978**, *50*, 725.
(28) Fekl, U.; Goldberg, K. I. *Adv. Inorg. Chem.* **2003**, *54*, 259.
(29) Lersch, M.; Tilset, M. *Chem. Rev.* **2005**, *105*, 2471.
(30) Stahl, S. S.; Labinger, J. A.; Bercaw, J. E. *Angew. Chem., Int. Ed.* **1998**, *37*, 2180.
(31) Bercaw, J. E.; Chen, G. S.; Labinger, J. A.; Lin, B. *J. Am. Chem. Soc.* **2008**, *130*, 17654.
(32) Bercaw, J. E.; Labinger, J. A. *Proc. Natl. Acad. Sci. U.S.A.* **2007**, *104*, 6899.
(33) Chen, G. S.; Labinger, J. A.; Bercaw, J. E. *Proc. Natl. Acad. Sci. U.S.A.* **2007**, *104*, 6915.
(34) Bartlett, K. L.; Goldberg, K. I.; Borden, W. T. *J. Am. Chem. Soc.* **2001**, *122*, 1456.
(35) Cowan, A. J.; Portius, P.; Kawanami, H. K.; Jina, O. S.; Grills, D. C.; Sun, X.-Z.; McMaster, J.; George, M. W. *Proc. Natl. Acad. Sci. U.S.A.* **2007**, *104*, 6933.
(36) Jones, W. D. *Inorg. Chem.* **2005**, *44*, 4475.
(37) Hall, C.; Perutz, R. N. *Chem. Rev.* **1996**, *96*, 3125.
(38) Schneider, J. J. *Angew. Chem., Int. Ed. Engl.* **1996**, *35*, 1068.
(39) Cobar, E. A.; Khaliullin, R. Z.; Bergman, R. G.; Head-Gordon, M. *Proc. Natl. Acad. Sci. U.S.A.* **2007**, *104*, 6963.
(40) Perutz, R. N.; Turner, J. J. *J. Am. Chem. Soc.* **1975**, *97*, 4791.
(41) Poliakoff, M.; Turner, J. J. *J. Chem. Soc., Dalton Trans.* **1974**, 2276.
(42) Bengali, A. A.; Schultz, R. H.; Moore, C. B.; Bergman, R. G. *J. Am. Chem. Soc.* **1994**, *116*, 9585.
(43) McNamara, B. K.; Yeston, J. S.; Bergman, R. G.; Moore, C. B. *J. Am. Chem. Soc.* **1999**, *121*, 6437.
(44) Childs, G. I.; Colley, C. S.; Dyer, J.; Grills, D. C.; Sun, X.-Z.; Yang, J. X.; George, M. W. *J. Chem. Soc., Dalton Trans.* **2000**, 1901.
(45) Ball, G. E.; Brookes, C. M.; Cowan, A. J.; Darwish, T. A.; George, M. W.; Kawanami, H. K.; Portius, P.; Rourke, J. P. *Proc. Natl. Acad. Sci. U.S.A.* **2007**, *104*, 6927.
(46) Calladine, J. A.; Torres, O.; Anstey, M.; Ball, G. E.; Bergman, R. G.; Curley, J.; Duckett, S. B.; George, M. W.; Gilson, A. I.; Lawes, D. J.; Perutz, R. N.; Sun, X.-Z.; Vollhardt, K. P. C. *Chem. Sci.* **2010**, *1*, 622.
(47) Calladine, J. A.; Vuong, K. Q.; Sun, X.-Z.; George, M. W. *Pure Appl. Chem.* **2009**, *81*, 1667.
(48) Geftakis, S.; Ball, G. E. *J. Am. Chem. Soc.* **1998**, *120*, 9953.
(49) Lawes, D. J.; Darwish, T. A.; Clark, T.; Harper, J. B.; Ball, G. E. *Angew. Chem., Int. Ed.* **2006**, *45*, 4486.
(50) Lawes, D. J.; Geftakis, S.; Ball, G. E. *J. Am. Chem. Soc.* **2005**, *127*, 4134.
(51) Calladine, J. A.; Duckett, S. B.; George, M. W.; Matthews, S. L.; Perutz, R. N.; Torres, O.; Vuong, K. Q. *J. Am. Chem. Soc.* **2011**, *133*, 2303.
(52) Young, R. D.; Hill, A. F.; Hillier, W.; Ball, G. E. *J. Am. Chem. Soc.* **2011**, *133*, 13806.
(53) Young, R. D.; Lawes, D. J.; Hill, A. F.; Ball, G. E. *J. Am. Chem. Soc.* **2012**, *134*, 8294.
(54) Castro-Rodriguez, I.; Nakai, H.; Gantzel, P.; Zakharov, L. N.; Rheingold, A. L.; Meyer, K. *J. Am. Chem. Soc.* **2003**, *125*, 15734.
(55) Evans, D. R.; Drovetskaya, T.; Bau, R.; Reed, C. A.; Boyd, P. D. W. *J. Am. Chem. Soc.* **1997**, *119*, 3633.
(56) Pike, S. D.; Thompson, A. L.; Algarra, A. G.; Apperley, D. C.; Macgregor, S. A.; Weller, A. S. *Science* **2012**, *337*, 1648.
(57) Bernskoetter, W. H.; Kloek Hanson, S.; Buzak, S. K.; Davis, Z.; White, P. S.; Swartz, R.; Goldberg, K. I.; Brookhart, M. *J. Am. Chem. Soc.* **2009**, *131*, 8603.
(58) Bernskoetter, W. H.; Schauer, C. K.; Goldberg, K. I.; Brookhart, M. *Science* **2009**, *326*, 553.
(59) Walter, M. D.; White, P. S.; Schauer, C. K.; Brookhart, M. *New J. Chem.* **2011**, *35*, 2884.
(60) Periana, R. A.; Bergman, R. G. *J. Am. Chem. Soc.* **1986**, *108*, 7332.
(61) Northcutt, T. O.; Wick, D. D.; Vetter, A. J.; Jones, W. D. *J. Am. Chem. Soc.* **2001**, *123*, 7257.
(62) Flood, T. C.; Janak, K. E.; Iimura, M.; Zhen, H. *J. Am. Chem. Soc.* **2000**, *122*, 6783.
(63) Jones, W. D. *Acc. Chem. Res.* **2003**, *36*, 140.
(64) DFT calculation of $\Delta G^{\ddagger}$ for the β-hydride elimination reaction to form the ethylene hydride complex using the same methodology described in the Experimental Section yields a value of 27.6 kcal/mol at 134 °C. The transition state for β-hydride elimination to form the ethylene hydride complex is the high point on the potential energy surface for the two-step reaction, which includes loss of ethylene (see SI for details).
(65) Mix, A.; Jutzi, P.; Rummel, B.; Hagedorn, K. *Organometallics* **2010**, *29*, 442.
(66) Ahlberg, P.; Harris, D. L.; Roberts, M.; Warner, P.; Seidl, P.; Sakai, M.; Cook, M.; Diaz, A.; Dirlam, J. P.; Hamberger, H.; Winstein, S. *J. Am. Chem. Soc.* **1972**, *94*, 7063.
(67) Anet, F. A. L.; Bourn, A. J. R. *J. Am. Chem. Soc.* **1967**, *89*, 760.
(68) Walter, M. D.; Moorhouse, R. A.; Urbin, S. A.; White, P. S.; Brookhart, M. *J. Am. Chem. Soc.* **2009**, *131*, 9055.
(69) Günther, H. *NMR Spectroscopy: Basic Principles, Concepts, and Application in Chemistry*; 2nd ed.; Wiley: Chichester, 1995.
(70) Schindler, M.; Kutzelnigg, W. *J. Am. Chem. Soc.* **1983**, *105*, 1360.
(71) Chan, B.; Ball, G. E. *J. Chem. Theory Comput.* **2013**, *9*, 2199.
(72) Flener-Lovitt, C.; Woon, D. E.; Dunning, T. H.; Girolami, G. S. *J. Phys. Chem. A* **2010**, *114*, 1843.
(73) Balcells, D.; Clot, E.; Eisenstein, O. *Chem Rev* **2010**, *110*, 749.
(74) Vastine, B. A.; Webster, C. E.; Hall, M. B. *J. Chem. Theory Comput.* **2007**, *3*, 2268.
(75) Casey, C. P.; Yi, C. S. *Organometallics* **1991**, *10*, 33.
(76) Findlater, M.; Cartwright-Sykes, A.; White, P. S.; Schauer, C. K.; Brookhart, M. *J. Am. Chem. Soc.* **2011**, *133*, 12274.
(77) Tempel, D. J.; Brookhart, M. *Organometallics* **1998**, *17*, 2290.
(78) Green, M. L. H.; Wong, L. L. *J. Chem. Soc., Chem. Commun.* **1988**, 677.
(79) Sandström, J. *Dynamic NMR Spectroscopy*; Academic Press: New York, 1982.
(80) Alaimo, P. J.; Peters, D. W.; Arnold, J.; Bergman, R. G. *J. Chem. Educ.* **2001**, *78*, 64.
(81) Pangborn, A. B.; Giardello, M. A.; Grubbs, R. H.; Rosen, R. K.; Timmers, F. J. *Organometallics* **1996**, *15*, 1518.
(82) Siegel, J. S.; Anet, F. A. L. *J. Org. Chem.* **1988**, *53*, 2629.
(83) Brookhart, M.; Grant, B.; Volpe, A. F. *Organometallics* **1992**, *11*, 3920.
(84) Andersen, R. A.; Wilkinson, G. *Inorg. Synth.* **1979**, *19*, 262.
(85) Frisch, M. J.; et al. *Gaussian 09*, revision B.01; Gaussian, Inc.: Wallingford CT, 2009.
(86) Andrae, D.; Häußermann, U.; Dolg, M.; Stoll, H.; Preuß, H. *Theor. Chim. Acta* **1990**, *77*, 123.
(87) Martin, J. M. L. S., A. *J. Chem. Phys.* **2001**, *114*, 3408.
(88) Perdew, J. P.; Burke, K.; Ernzerhof, M. *Phys. Rev. Lett.* **1996**, *77*, 3865.
(89) Ghosh, R.; Zhang, X.; Achord, P.; Emge, T. J.; Krogh-Jesperson, K.; Goldman, A. S. *J. Am. Chem. Soc.* **2007**, *129*, 853.
(90) Quintal, M. M.; Karton, A.; Iron, M. A.; Boese, A. D.; L., M. J. M. *J. Phys. Chem. A* **2006**, *110*, 709.
(91) Montag, M.; Efremenko, I.; Cohen, R.; Leitus, G.; Shimon, L. J. W.; Diskin-Posner, Y.; Ben-David, Y.; Martin, J. M. L.; Milstein, D. *Chem.—Eur. J.* **2008**, *14*, 8183.